Magnetoelectric phenomena in Fe langasites

A. Yu. Tikhanovskii,[1,2,*] V. Yu. Ivanov,[1] A. M. Kuzmenko,[1] A. M. Balbashov,[3,†] Z. Wang,[4] V. Skumryev,[5] and A. A. Mukhin[1,‡]

[1]*Prokhorov General Physics Institute, Russian Academy of Sciences, Moscow 119991, Russia*
[2]*Moscow Institute of Physics and Technology (State University), Moscow Region 141700, Russia*
[3]*Moscow Power Engineering Institute, Moscow 111250, Russia*
[4]*Hochfeld-Magnetlabor Dresden, Helmholtz-Zentrum, Dresden-Rossendorf D-01314, Germany and Anhui Province Key Laboratory of Condensed Matter Physics at Extreme Conditions, High Magnetic Field Laboratory of the Chinese Academy of Sciences, Hefei 230031, China*
[5]*Departament de Física, Universitat Autònoma de Barcelona, 08193 Bellaterra, Barcelona, Spain and Institució Catalana de Recerca i Estudis Avançats, 08010 Barcelona, Spain*

(Received 28 November 2021; accepted 4 March 2022; published 25 March 2022)

Experimental and theoretical studies of the magnetoelectric properties of a series of Fe langasite multiferroics ($Ba_3NbFe_3Si_2O_{14}$, $Ba_3TaFe_3Si_2O_{14}$, and $Sr_3TaFe_3Si_2O_{14}$) with planar triangular spiral magnetic structure and double chiral magnetic order have been carried out. Magnetic field induced electric polarization is observed to emerge in the basal ab^* plane of the trigonal crystal, depending on both the magnitude (up to 60 T) and orientation of the magnetic field. Remarkably, the induced polarization is very sensitive to the projection of the field onto the c axis, with a sharp increase in polarization found for small deviations of the field from the basal plane and the sign of polarization determined by the direction of the field deviation. At high magnetic fields, the electric polarization behavior changes qualitatively and strongly depends on the magnetic field orientation. A detailed group theoretical analysis of the magnetic and magnetoelectric properties of Fe langasites is presented, and a relationship between the polarization and magnetic order parameters in an external magnetic field is established. We show that, in a magnetic field, the spiral magnetic structure is rotated and canted with respect to the original structure under zero field. The competition between these two processes, rotation and canting, strongly depends on the magnetic field orientation, and determines the polarization behavior. We propose a simplified description of the Fe langasites' triangular spiral magnetic structure at low temperatures and with saturated moments, characterized by the spiral plane orientation and the field-induced magnetization only. We establish that, at weak fields, the appearance of polarization occurs mainly due to the reorientation of the magnetic spiral (analogous to a spin-flop transition) and could be explained by the inverse Dzyaloshinskii-Moriya interaction. At high fields (above 8 T), the polarization change occurs via canting of the magnetic spiral, owing to Fe-Fe exchange and single-ion contributions.

DOI: 10.1103/PhysRevB.105.104424

I. INTRODUCTION

In recent years multiferroic materials with coexisting, different types of orderings (i.e., electric, magnetic, etc.) have been intensively studied [1–5]. They offer a possibility to change electric polarization by magnetic field or, conversely, to control magnetic properties by applying electric field [6–8]. The magnetoelectric effect can be used in spintronics for highly efficient control of magnetization by external electric field since no energy losses for the creation of a magnetic field by electric current are involved. However, most commonly, electric and magnetic properties are weakly coupled with each other and rarely coexist in the same material [2,9]. Therefore, the search for multiferroics with strong magnetoelectric coupling remains a challenge. Compounds belonging to the so-called group of langasites La_3Ga_5SiO [10] are interesting materials in this respect. They also exhibit large piezoelectric and nonlinear optical effects [11–13].

Recently, iron-containing langasites ($Ba_3NbFe_3Si_2O_{14}$, $Ba_3TaFe_3Si_2O_{14}$, and $Sr_3TaFe_3Si_2O_{14}$), which are emerging as a new class of compounds exhibiting magnetoelectric properties [14,15], were synthesized. They have attracted attention due to their nontrivial magnetic structure and the presence of magnetoelectric effect [16–18].

The Fe-langasite structure belongs to the noncentrosymmetric P321 space group. The only magnetic ions Fe^{3+} with spin $S = 5/2$ occupy three nonequivalent positions $3f$ of C_2 symmetry, with local twofold axes at 120° to each other and lying along the crystallographic directions a, b, and $-a$–b [Fig 1(a)]. Below $T_N = 27$ K, they order antiferromagnetically into a structure with double chirality. The structure is characterized by (a) in-plane (in ab) rotation of spins in positions 1, 2, and 3 with anticlockwise or clockwise rotation angles $\epsilon_T 2\pi/3$, where $\epsilon_T = \pm 1$ specifies the direction of rotation in a "triangular" structure [Fig. 2(a)] [19], and (b) rotation of

*tikhanovskii@phystech.edu
†Deceased.
‡mukhin@ran.gpi.ru

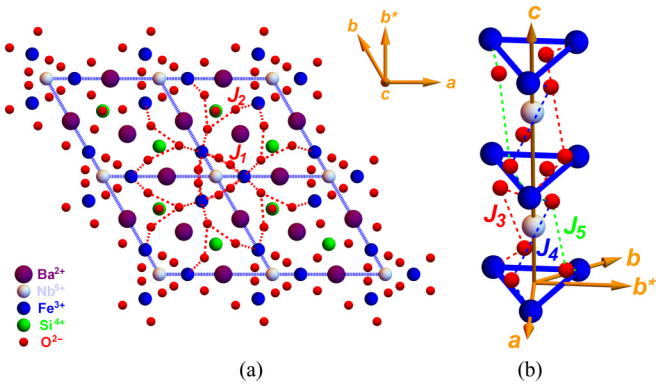

FIG. 1. (a) The left-handed [14] crystal structure of $Ba_3NbFe_3Si_2O_{14}$ in projection on the basal plane (*ab*); the red dashed lines represent the paths of in-plane exchange interactions J_1 and J_2 between Fe^{3+} ions. (b) The interplanar Fe-Fe exchange interactions J_3, J_4, and J_5 are represented in red, blue, and green, respectively (for the left-handed crystal $J_5 > J_3$ and corresponding parameter $\epsilon_{St} = \text{sign}(J_5 - J_3) = +1$).

the spins along the *c* axis with a wave vector $k \approx (0, 0, \pm 1/7)$ [Fig. 2(b)] [14,15,20].

In exchange approximation, the Hamiltonian $H = \sum_{mv,l\mu} J_{mvl\mu} \mathbf{S}_v(\boldsymbol{k}, \boldsymbol{r}_m) \boldsymbol{S}_\mu(\boldsymbol{k}, \boldsymbol{r}_l)$ (where ν and μ are the in-plane unit cell position numbers, and m and l are the unit cell numbers), and also the interaction between magnetic Fe^{3+} ions is described by five exchange interactions $J_1, \ldots, J_5$ [14,15]. The superexchange interaction J_1 occurs through one O^{2-} atom, while $J_2, \ldots, J_5$ occur through two O^{2-} atoms and are of super-superexchange type. The in-plane interactions J_1 and J_2 [Fig. 1(a)] are the strongest ($J_1 \approx 1.6$ meV and $J_2 \approx 0.31$ meV [21]), and minimization renders a 120° (triangular) arrangement of the in-plane spins [Fig. 2(a)]. The three nonequivalent interplane interactions J_3, J_4, and

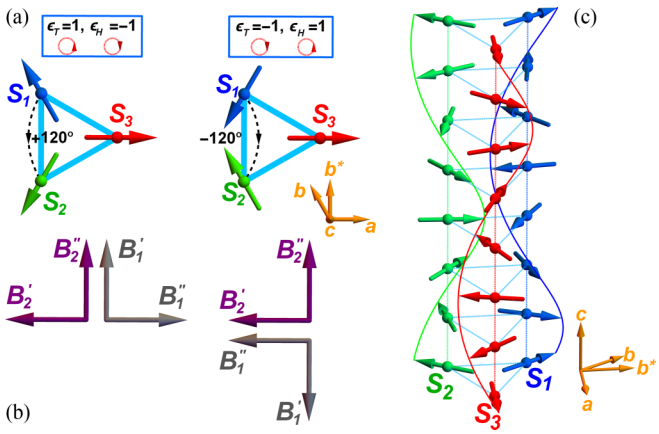

FIG. 2. (a) Magnetic structure of Fe^{3+} ions in left-handed ($\epsilon_{St} = 1$) crystal $Ba_3NbFe_3Si_2O_{14}$ for the three Fe positions 1, 2, and 3 in the *ab* plane placed at angle $-120°$ ($\epsilon_T = -1$, right) or $+120°$ ($\epsilon_T = 1$, left), and (b) imaginary ($\boldsymbol{B}_i''$) and real ($\boldsymbol{B}_i'$) components of vectors $\boldsymbol{B}_1$ and $\boldsymbol{B}_2$. (c) General view of moment's distribution in the three nonequivalent positions for $\epsilon_T = 1$, $\epsilon_H = -1$ with the corresponding envelope curves, which form a planar triangular magnetic spiral with a wave vector $\boldsymbol{k} \approx (0, 0, 1/7\epsilon_H)$.

J_5 [Fig. 1(b)] are responsible for the incommensurate spiral structure along the *c* axis, with a wave vector $k \approx (0.0, \pm 1/7)$ [Fig. 2(b)].

Besides the strong exchange interactions, there are also weaker magnetic interactions in the Fe langasites, which lead to additional distortions of the magnetic structure. It was shown [22] that local (single-ion) anisotropy exists at the $3f$ positions of the Fe^{3+} ions with an easy axis along the second-order axes *a*, *b*, and *–a–b*. It leads to a distortion of the magnetic spiral (spin bunching) and influences the magnetic chirality [19]. Dzyaloshinskii-Moriya interaction is also present in the Fe langasites [21,23] which results in deviation of magnetic moments from the basal plane at low temperatures and additional modulation of the magnetic structure along the *c* axis, called a "helical butterfly" [24].

The Fe-langasite space group is compatible with magnetoelectric effect existence, as reported in several works. Nevertheless, recent studies turned out to be contradictory. The authors of [14] reported spontaneous polarization ($\sim 9\ \mu C/m^2$) along the *c* axis; this value was supported also by density functional theory (DFT) calculations [25]. However, the spontaneous polarization was not confirmed by other studies. In particular, electric polarization was found only as induced by magnetic field in the *ab* plane or at small deviations from it [16,26]. The effect was attributed [26] to the inverse Dzyaloshinskii-Moriya interaction [27]. On the other hand, in a recent paper [28], was pointed out that the field-induced polarization in the basal plane is related to structural chirality, as well as to the distortions of the 120° magnetic structure by the field and the long-wave modulation of the spins in the basal plane. Thus, there are certain contradictions in the known experimental data on the magnetoelectric effect in Fe langasites. There is still no univocal understanding of its mechanisms and the conditions for its manifestation in the field and the orientation properties of the electric polarization.

In this article, we investigate magnetoelectric properties of $Ba_3NbFe_3Si_2O_{14}$, $Ba_3TaFe_3Si_2O_{14}$, and $Sr_3TaFe_3Si_2O_{14}$ single crystals in a wide range of magnetic fields (up to 60 T). A strong dependence of magnetoelectric properties on the field orientation relative to the crystallographic axes is established. Based on a phenomenological approach, which takes into account the crystal symmetry, we propose a simplified description of Fe langasites' complex spiral magnetic structure. We describe spiral structure evolution in the magnetic field, and analyze the mechanisms of field-induced electric polarization. Since the preliminary studies indicated that all the magnetoelectric features of the three langasites under study are practically the same, $Ba_3NbFe_3Si_2O_{14}$ was studied in more detail and reported as representative.

II. METHODS

$Ba_3NbFe_3Si_2O_{14}$, $Ba_3TaFe_3Si_2O_{14}$, and $Sr_3TaFe_3Si_2O_{14}$ single crystals were grown by floating-zone melting with radiation heating [29,30]. The x-ray analysis confirmed the presence of a single-phase structure belonging to the *P*321 space group; the orientation of the crystals was determined by the Laue method. The magnetic properties were studied by the MPMS-50 (Quantum Design) in fields up to 5 T and at temperatures from 2 to 300 K. Pyroelectric studies were

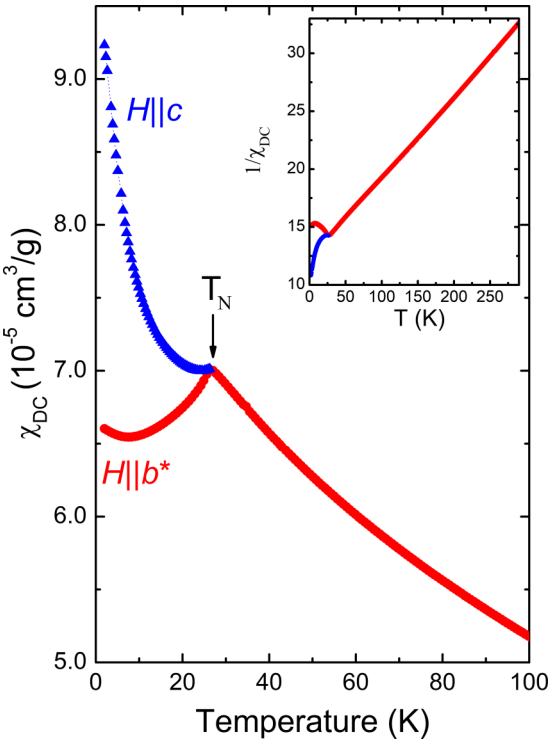

FIG. 3. Temperature dependences of DC susceptibility in $Ba_3NbFe_3Si_2O_{14}$ along the crystallographic directions b^* (red symbols) and c (blue symbols) measured in field $\mu_0 H = 0.1$ T. The susceptibility along the a axis coincides with the one along the b^* axis. Inset: inverse susceptibility along b^* (red) and c (blue) axes as a function of temperature in a wide range.

performed using a Keithley 6517A electrometer in static fields (in an electromagnet up to 1.4 T, in MPMS up to 5 T, and in a cryocooler cryogen-free system up to 8 T). Magnetoelectric measurements were also carried out in pulsed fields up to 60 T with a pulse duration of 200 ms at the Dresden High Magnetic Fields Laboratory. Dielectric polarization P was measured by a pyroelectric technique [31]. The pyrocurrent was captured through the voltage variation in a shunt resistor connected in series with the measurement circuit by a digital oscilloscope Yokogawa DL750 with a high sampling rate of 1 MS s^{-1} and a resolution of 16 bits. Then P was calculated by integrating the pyrocurrent numerically. The accuracy of the sample's orientation in the high field experiment was about 2°–5°. No effect on the electric polarization was observed when cooling the samples from temperatures exceeding T_N in an external electric field. Therefore, all measurements were performed without poling the samples.

III. EXPERIMENT

Temperature dependence of the DC susceptibility $\chi = \sigma/H$ measured in a field of 0.1 T for $Ba_3NbFe_3Si_2O_{14}$ is shown in Fig. 3. It demonstrates an anomaly at $T_N \approx 27$ K above which the magnetic susceptibility obeys the Curie-Weiss law and does not show anisotropy, while below T_N the anisotropy of the susceptibility in the basal plane and along the c axis is noticeable. The susceptibility anisotropy decreases with increasing magnetic field, as illustrated by the

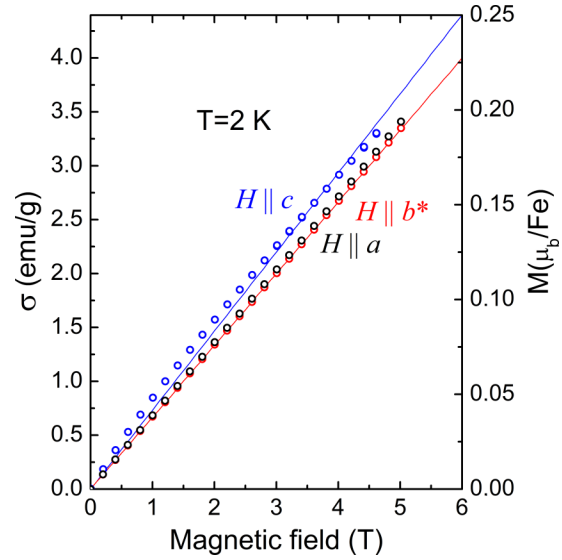

FIG. 4. Magnetization curves along c axis (blue), a axis (black), and b^* (red) at 2 K. Symbols: experiment; lines: model simulations (see text). Magnetization along a and b^* axes practically coincide.

magnetization curves $\sigma(H)$ measured at temperatures $T < T_N$ (Fig. 4). In a field applied within the basal plane $\sigma(H)$ remains linear, while for $H||c$ there is a slight deviation from the linear dependence in fields $H < 2$ T. The results agree with the previously published data [15,16].

No spontaneous electric polarization was observed along the main crystallographic directions (a, b^*, c) by pyroelectric temperature measurements (within an accuracy of $\sim 1\ \mu C/m^2$) at 2 K.

Measurements of the angular dependences of the electric polarization in a small magnetic field of about 1.4 T allowed finding the symmetry conditions for inducing it. In particular, the polarization along the a axis (P_a) emerges when the field H rotates in the b^*c plane and is proportional to $\sin(2\theta_H)$ [Fig. 5(a)], where θ_H is an angle between the H direction and the ab^* plane. P_a is absent (with an accuracy of $\sim 0.1\ \mu C/m^2$) when H rotates in the ab^* and ac planes. Similarly, the polarization in the orthogonal direction $P_{b^*} \sim \sin(2\theta_H)$, but it appears when H is in the orthogonal ac plane [Fig. 5(b)] and is absent when H rotates in the ab^* and b^*c planes. In this field range the observed values of P_a and P_{b^*} are proportional to the square of the magnetic field [Fig. 5(c)]. As to the polarization along the c axis, it is absent (within the experimental accuracy) for all orientations of the field.

Considering the spiral magnetic structure in the studied system, the inverse Dzyaloshinskii-Moriya interaction emerges as one of the possible mechanisms behind the observed magnetoelectric effect. According to Ref. [7], it determines the electric polarization $\boldsymbol{P} \sim \boldsymbol{n} \times \boldsymbol{k}$, where $\boldsymbol{k} = (0, 0, k)$ is the wave vector of the magnetic helix, and $\boldsymbol{n} \sim \boldsymbol{S}_i \times \boldsymbol{S}_{i+1}$ is the spin-rotation axis being normal to the spin helix plane, determined by its chirality ($\boldsymbol{S}_i$ and $\boldsymbol{S}_{i+1}$ are the spins of Fe in the i and $i+1$ helix planes). Since $\boldsymbol{n}||\boldsymbol{k}$ in $H = 0$, there is no spontaneous polarization, and a deviation of $\boldsymbol{n}$ from $\boldsymbol{k}$ (c axis) is required for it to appear. Due to the absence of net magnetic moment, the spin-rotation axis $\boldsymbol{n}$ does

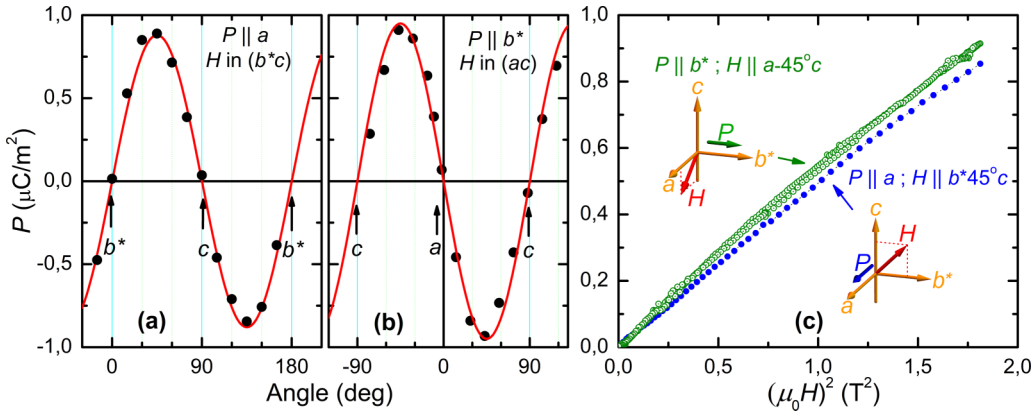

FIG. 5. Angular dependencies of the electric polarization P (a) along a axis in magnetic field applied in b^*c plane, and (b) along b^* axis in field within ac plane [black points: experiment; red lines: fit by $\sin(2\theta_H)$, where θ_H is the angle between the field and the basal plane]. The applied field is ~1.4 T and temperature is 4.2 K. (c) P_a and P_{b^*} components of polarization versus square of magnetic field applied along different directions indicated in the insets.

not deviate from the c axis in small fields, either for $H||c$ or $H\perp c$. Deviation of $\boldsymbol{n}$ (i.e., $n_{x,y}$ appearance) could occur only in the presence of both H_z and $H_{x,y}$ field's components, which provide torque due to the anisotropy of the magnetic susceptibility parallel ($\chi_{||}$) and perpendicular ($\chi_\perp$) to the plane of the spin spiral and nonzero $\Delta\chi = \chi_\perp - \chi_{||}$. On the other hand, the crystallographic magnetic anisotropy KS_{zi}^2 stabilizes the basal ab^* plane and opposes the deviation. Therefore, the plane deviation is determined by the balance of these two factors, $n_{x,y} \sim \Delta\chi H_z H_{x,y}/K$. Thus, when the helix spin-rotation axis n deviates from the wave vector, polarization $P_x \sim n_y k \sim H_y H_z k$ and $P_y \sim -n_x k \sim -H_x H_z k$ appears and produces the observed angular dependence $\sim H^2 \sin 2\theta_H$ (Fig. 5). In addition to inverse Dzyaloshinskii-Moriya interaction, the noncentrosymmetric trigonal crystal lattice symmetry of the Fe langasites allows a magnetic field induced quadratic contribution to the electric polarization (analogous to *pd* hybridization [32–34]). Such mechanism is not directly associated with the magnetic structure and was previously observed in trigonal rare-earth iron borates [35], aluminum borates [36], and recently in rare-earth langasites [37]. In these systems, an external magnetic field induces electric polarization, which manifests itself in the quadratic magnetization terms $P_x \sim \beta_1 M_y M_z + \beta_2 (M_x^2 - M_y^2)$, $P_y \sim -\beta_1 M_x M_z - 2\beta_2 M_x M_y$, where $\boldsymbol{M} = (M_x; M_y; M_z)$ is the magnetization of the system, and β_1 and β_2 are magnetoelectric constants [35,36]. Since in low fields $M_{x,y,z} \sim H_{x,y,z}$, the terms $\beta_1 M_y M_z$ and $-\beta_1 M_x M_z$ will be proportional to $H^2 \sin(2\theta_H)$, which is also in agreement with the observed angular dependences. According to the experimental dependences [Figs. 5(a) and 5(b)], the role of the terms $\beta_2(M_x^2 - M_y^2)$ and $-2\beta_2 M_x M_y$, having another angular dependence $\sim \cos^2\theta_H$, is insignificant in weak fields. Thus, the angular dependences of polarization in small fields are qualitatively consistent with both mechanisms described above (i.e., the inverse Dzyaloshinskii-Moriya interaction and field-induced magnetization). Hence, high field measurements are required for their separation.

The electric polarization features obtained in weak fields were confirmed in fields up to 8 T. In particular, the polarization along the c axis (P_c) was negligible for all directions of the magnetic field. No polarization along the a and b^* axes was observed (within the accuracy of $\sim 0.2\ \mu C/m^2$) for the field along the c axis.

Electric polarization, measured along the a or b^* axes, is found to be very sensitive to the presence of the external magnetic field component along the c axis (Fig. 6). With slight controlled deviations of the magnetic field from the basal plane at nominal angles (accuracy in orientation $\approx \pm 3^\circ$), $\theta_H = +9^\circ$ and -3° in Figs. 6(a) and 6(b), the polarization remains small up to critical fields of about 4–6 T, after which a sharp increase up to values over $8\ \mu C/m^2$ occurs. This is associated with the magnetic spiral reorientation to the direction almost perpendicular to the magnetic field (see below). In small fields, deviated from the basal plane by nominal angles $\theta_H \sim \pm 45^\circ$, the polarization quadratically increases while its field dependence changes above ~5 T. This feature could be associated with a change of interrelation between the two contributions, i.e., the inverse Dzyaloshinskii-Moriya interaction determined by the orientation of the spin helix and the field-induced magnetization $\beta_1 M_y M_z$ and $-\beta_1 M_x M_z$ [Figs. 6(a)–6(c)].

We note that for all studied geometries $P_a(H_{b^*\theta c})$ [Fig. 6(a)], $P_{b*}(H_{a\theta c})$ [Fig. 6(b)], and $P_a(H_{a45b^*\theta c})$ [Fig. 6(c)] the relation $P(\theta_H) \approx -P(-\theta_H)$ is fulfilled in fields up to 6 T; i.e., when the magnetic field projection on the c axis changes sign, the polarization sign also changes. This results from the change of the magnetic helix plane reorientation direction. Above 6 T, this rule is somewhat violated for nominal angles $\theta_H = +45^\circ$ and -45° in the $P_a(H_{b^*\theta c})$ geometries, since there is a slight asymmetry in the polarization curves. At lower nominal angles $\theta_H = +9^\circ$ and -3°, the $P_a(H_{b^*\theta c})$ curves [Fig. 6(a)] become very different from the $P_{b^*}(H_{a\theta c})$ ones [Fig. 6(b)], which Is due to the quadratic contribution $\beta_2(M_x^2 - M_y^2)$. We obtained more symmetric dependences [see Fig. 6(c), $\theta_H = \pm 5^\circ$] for the $P_a(H_{a45b^*\theta c})$ geometries where the field projection lies along the diagonal of the ab^* plane ($M_x = M_y$) and the contribution $\beta_2(M_x^2 - M_y^2)$ to the polarization is absent.

In pulsed fields up to 60 T, we found stronger contributions to polarization associated with the induced magnetization. It is primarily manifested in the violation of the relationship $P(\theta_H) \approx -P(-\theta_H)$ and qualitative changes in the field

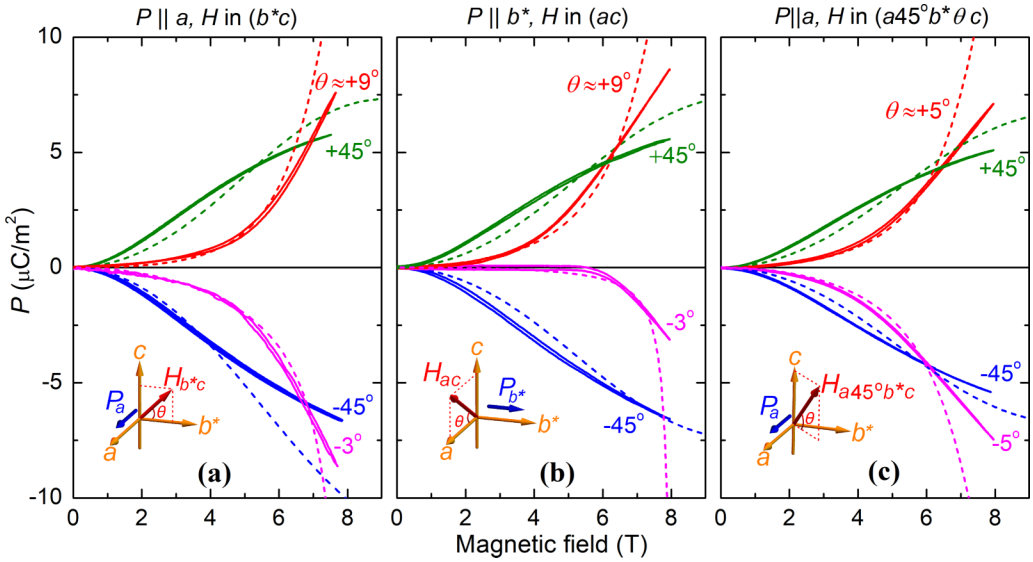

FIG. 6. Dependencies of the a and b^* components of the electric polarization on magnetic field $\boldsymbol{H}$ in different orientations with respect to the crystal axes ($T = 9$ K): (a) $P_a(H_{b^*\theta c})$, (b) $P_{b^*}(H_{a\theta c})$, (c) $P_a(H_{a45b^*\theta c})$. The cumbersome subscript in the magnetic field denotes its orientation, for example, $H_{a45b^*\theta c}$ indicates that the field deviates from the ab^* plane at an angle θ_H towards the c axis in the vertical plane crossing the ab^* plane at an angle of 45° to the a axis. Note that the values θ_H are nominal (accuracy in orientation ≈±3°). The insets show the corresponding orientations of the magnetic field vector and the polarization. At small deviations of the field from the basal plane, a sharp increase of polarization occurs which is associated with the triangular spiral magnetic structure reorientation perpendicular to the field. Solid lines: experiment; dotted lines: model simulations (see text).

dependences [Figs. 7(a)–7(c)]. This is most clearly seen in the $P_a(H_{b^*\pm 10c})$ geometries, for which the quadratic contribution $\beta_2(M_x^2 - M_y^2)$ leads to a drastic decrease (up to –170 μC/m^2) of the polarization, regardless of the magnetic field projection (±10°) [Fig. 7(a)]. On the contrary, we expected symmetric curves for geometries $P_a(H_{a45b^*\pm 10c})$ when the field projection lies along the diagonal of the ab^* plane ($M_x = M_y$), and this quadratic contribution should be absent. However, there is still quadric contribution in polarization [Fig. 7(b)], which we attribute to slight field deviation from the diagonal of the ab^* plane due to possible sample misalignment. Interestingly, the contributions associated with the induced magnetization

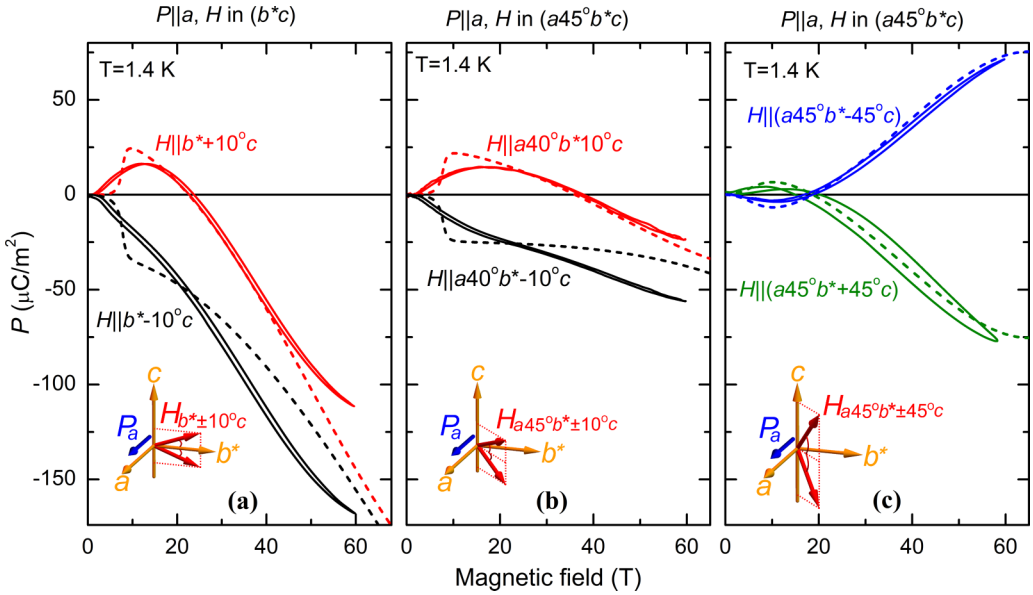

FIG. 7. Dependencies of the electric polarization on a pulsed magnetic field up to 60 T in different orientations with respect to the crystallographic axes ($T = 1.4$ K): (a) $P_a(H_{b^*\pm 10c})$, (b) $P_a(H_{a45b^*\pm 10c})$, and (c) $P_a(H_{a45b^*\pm 45c})$, where notations of the complex subscript in the magnetic field are similar to ones in the Fig. 6 caption. The insets show the corresponding orientations of the magnetic field and the polarization. Solid lines: experiment; the dashed lines: model simulations (see text).

strongly depend on the field deviation θ_H from the basal plane [Figs. 7(b) and 7(c)].

Thus, we revealed qualitatively different behavior of the polarization depending on the orientation and magnitude of the magnetic field. It could be due to a competition between different contributions associated with a reorientation of the spiral spin structure (via inverse Dzyaloshinskii-Moriya interaction) and the field-induced magnetization.

IV. THEORY AND DISCUSSION

In this section, we will introduce magnetic order parameters describing the evolution of the magnetic structure of Fe langasites in a magnetic field. Next we construct a nonequilibrium phenomenological thermodynamic potential, the minimum of which gives the equilibrium value of the order parameters, and analyze the magnetization curves. Then, based on the symmetry of the system, the relationship of the electric polarization in the ab^* plane ($P_{x,y}$) and the order parameters is established and the observed dependences of polarization in the magnetic field are analyzed. A simplified (reduced) description of the Fe langasites' behavior in the low temperature region, when the magnetic moments are saturated, is proposed.

A. Magnetic order parameters

Fe-langasite crystal structure belongs to the $P321$ noncentrosymmetric space group. Fe^{3+} magnetic ions (spin 5/2) occupy three nonequivalent $3f$ positions in the basal plane [14,15]. Each of these positions is characterized by a spin $\boldsymbol{S}_\nu(\boldsymbol{k}, \boldsymbol{r}_m)$ where $\nu = 1, 2, 3$ determines its site in the triangle; $\boldsymbol{r}_m$ is a position of triangle m along the c axis (Fig. 2); and $\boldsymbol{k} = (0, 0, k)$ is a wave vector of the spin helix.

Dominant isotropic exchange interactions form a helicoidal magnetic structure with a wave vector $\boldsymbol{k}$ in Fe langasites [14], [15]. Thus, the spin of the magnetic helix plane $\boldsymbol{r}_m$ is represented as a Fourier transformation with a given wave vector: $\boldsymbol{S}_\nu(\boldsymbol{k}, \boldsymbol{r}_m) = \boldsymbol{S}_{\nu\boldsymbol{k}} e^{i\boldsymbol{k}\boldsymbol{r}_m} + \boldsymbol{S}^*_{\nu\boldsymbol{k}} e^{-i\boldsymbol{k}\boldsymbol{r}_m}$ [38,39]. In general, taking into account three nonequivalent positions ν, the system is characterized by 18 order parameters: imaginary and real components of the vectors $\boldsymbol{S}_{\nu\boldsymbol{k}}$.

To describe the magnetic behavior of the Fe langasites in a frame of k vector's little group, it is convenient to use symmetrized combinations of the spin order parameters $\boldsymbol{S}_{1\boldsymbol{k}}$, $\boldsymbol{S}_{2\boldsymbol{k}}$, $\boldsymbol{S}_{3\boldsymbol{k}}$ in three nonequivalent sites (spirals), namely, ferro- ($\boldsymbol{F}$) and antiferromagnetic ($\boldsymbol{B}_{1,2}$) vectors:

$$\begin{aligned} \boldsymbol{F} &= \boldsymbol{S}_{1\boldsymbol{k}} + \boldsymbol{S}_{2\boldsymbol{k}} + \boldsymbol{S}_{3\boldsymbol{k}}, \\ \boldsymbol{B}_1 &= \sqrt{3}(\boldsymbol{S}_{1\boldsymbol{k}} - \boldsymbol{S}_{2\boldsymbol{k}}), \\ \boldsymbol{B}_2 &= \boldsymbol{S}_{1\boldsymbol{k}} + \boldsymbol{S}_{2\boldsymbol{k}} - 2\boldsymbol{S}_{3\boldsymbol{k}}. \end{aligned} \tag{1}$$

Taking into account the spiral magnetic structure, we introduce a cyclic coordinate system. In this case, the νth position spin's Fourier component is represented as

$$\boldsymbol{S}_{\nu\boldsymbol{k}} = S_{\nu\boldsymbol{k}(+1)}\mathbf{e}^{+1} + S_{\nu\boldsymbol{k}(0)}\mathbf{e}^{0} + S_{\nu\boldsymbol{k}(-1)}\mathbf{e}^{-1}, \tag{2a}$$

where $\mathbf{e}^{+1} = -(\mathbf{e}_x - i\mathbf{e}_y)/\sqrt{2}$, $\mathbf{e}^0 = \mathbf{e}_z$, $\mathbf{e}^{-1} = (\mathbf{e}_x + i\mathbf{e}_y)/\sqrt{2}$ are covariant unit vectors in terms of orthogonal ones $\mathbf{e}_{x,y,z}$, and $S_{\nu\boldsymbol{k}(+1)} = -(S_{\nu\boldsymbol{k}(\mathrm{x})} + iS_{\nu\boldsymbol{k}(\mathrm{y})})/\sqrt{2}$, $S_{\nu\boldsymbol{k}(0)} = S_{\nu\boldsymbol{k}(z)}$, $S_{\nu\boldsymbol{k}(-1)} = (S_{\nu\boldsymbol{k}(\mathrm{x})} - iS_{\nu\boldsymbol{k}(\mathrm{y})})/\sqrt{2}$ are contravariant spin components in terms of their usual components $S_{\nu\boldsymbol{k}(x,y,z)}$ in an orthogonal coordinate frame [40]. Symmetrized order parameters $\boldsymbol{F}$, $\boldsymbol{B}_1$ $\boldsymbol{B}_1$, and $\boldsymbol{B}_2$ have a similar form in a cyclic coordinate system.

Table I, obtained using the Bilbao crystallographic server [41], represent the order parameters $\boldsymbol{F}$, $\boldsymbol{B}_1$, and $\boldsymbol{B}_2$ transformation properties in the $\boldsymbol{k} = (0, 0, \pm k)$ group, which include the symmetry elements $\{3_c\}$ and $\{2_a\}$. We note that exactly ferromagnetic components,

$$\begin{aligned} F_{(0)}\mathbf{e}^0 &= \sum_\nu S_{\nu\boldsymbol{k}(\mathrm{z})}\mathbf{e}_\mathrm{z}, \\ F_{(\pm1)}\mathbf{e}^{\pm1} &= \frac{1}{2}\sum_\nu (S_{\nu\boldsymbol{k}(\mathrm{x})} \pm iS_{\nu\boldsymbol{k}(\mathrm{y})})(\mathbf{e}_\mathrm{x} \mp i\mathbf{e}_\mathrm{y}), \end{aligned} \tag{2b}$$

and combinations of the antiferromagnetic vectors components,

$$\begin{aligned} (\boldsymbol{B}_2 \pm i\boldsymbol{B}_1)_{(0)}\mathbf{e}^0 &= [(S_{1\boldsymbol{k}(z)} + S_{2\boldsymbol{k}(z)} - 2S_{3\boldsymbol{k}(z)}) \pm i\sqrt{3}(S_{1\boldsymbol{k}(z)} - S_{2\boldsymbol{k}(z)})]\mathbf{e}_z \\ (\boldsymbol{B}_2 \pm i\boldsymbol{B}_1)_{(\pm1)}\mathbf{e}^{\pm1} &= \frac{1}{2}[\{(S_{1\boldsymbol{k}(x)} + S_{2\boldsymbol{k}(x)} - 2S_{3\boldsymbol{k}(x)}) \pm i(S_{1\boldsymbol{k}(y)} + S_{2\boldsymbol{k}(y)} - 2S_{3\boldsymbol{k}(y)})\} \\ &\quad \pm i\sqrt{3}\{(S_{1\boldsymbol{k}(x)} - S_{2\boldsymbol{k}(x)}) \pm i(S_{1\boldsymbol{k}(y)} - S_{2\boldsymbol{k}(y)})\}](\mathbf{e}_x \mp i\mathbf{e}_y), \end{aligned} \tag{2c}$$

in a cyclic basis transform according to three different two-dimensional representations, DT1–DT3.

We consider the main types of magnetic structures arising in exchange approximation. Based on Table I, one can find invariant quadratic combinations of the order parameters $\boldsymbol{F}$ and $\boldsymbol{B}_{1,2}$ and construct the thermodynamic potential in the exchange approximation:

$$\begin{aligned} \Phi_0 &= \alpha_M|\boldsymbol{F}|^2 + \beta_+[|(\boldsymbol{B}_2 + i\boldsymbol{B}_1)_{(+1)}|^2 + |(\boldsymbol{B}_2 + i\boldsymbol{B}_1)_{(-1)}|^2 - |(\boldsymbol{B}_2 + i\boldsymbol{B}_1)_{(0)}|^2] \\ &\quad + \beta_-[|(\boldsymbol{B}_2 - i\boldsymbol{B}_1)_{(+1)}|^2 + |(\boldsymbol{B}_2 - i\boldsymbol{B}_1)_{(-1)}|^2 - |(\boldsymbol{B}_2 - i\boldsymbol{B}_1)_{(0)}|^2] + \cdots \\ &= \alpha_M|\boldsymbol{F}|^2 + (\beta_+ + \beta_-)(|\boldsymbol{B}_1|^2 + |\boldsymbol{B}_2|^2) + i(\beta_+ - \beta_-)(\boldsymbol{B}_1\boldsymbol{B}_2{}^* - \boldsymbol{B}_1{}^*\boldsymbol{B}_2) + \cdots, \end{aligned} \tag{3}$$

where α_M, $\beta_\pm$ are phenomenological constants. Thus, in exchange approximation, the order parameters $\boldsymbol{F}$ and $\boldsymbol{B}_{1,2}$ are independent and correspond to two spin structures in the group of wave vector $\boldsymbol{k}$. One (with $\boldsymbol{F} \neq \boldsymbol{0}$ and $\boldsymbol{B}_{1,2} = 0$) corresponds to the helicoidal structures in three nonequivalent positions of Fe^{3+} with a parallel spins orientation in the spiral

TABLE I. Irreducible (two-dimensional) representations of the $\boldsymbol{k} = (0, 0, \pm k)$ wave vector group of the P321 space group and transformation properties of the symmetrized combinations $\boldsymbol{F} = \boldsymbol{S}_{1k} + \boldsymbol{S}_{2k} + \boldsymbol{S}_{3k}$, $\boldsymbol{B}_1 = \sqrt{3}(\boldsymbol{S}_{1k}–\boldsymbol{S}_{2k})$, $\boldsymbol{B}_2 = \boldsymbol{S}_{1k} + \boldsymbol{S}_{2k}–2\boldsymbol{S}_{3k}$ of spin Fourier components and their complex conjugated parts in $3f$ sites. The complex components $\boldsymbol{F}$, $\boldsymbol{B}_2 \pm i\boldsymbol{B}_1$ are given in a cyclic basis. The last column represents these order parameters in a frame of reduced description in terms of the polar (ω) and azimuthal (φ) angles of the real part of $\boldsymbol{B}_2$ for the left-handed enantiomorphic crystal modification with $J_5 > J_3$ and the triangular chirality $\epsilon_T = +1$ that determines the helix chirality $\epsilon_H = -\epsilon_T\epsilon_{St}$; $a = \exp[2\pi i/3]$ and $a^* = \exp[–2\pi i/3]$.

	Matrices of the representations of the group			$\boldsymbol{F}$ components in cyclic basis	$\boldsymbol{B}_2 \pm i\boldsymbol{B}_1$ components in cyclic basis		Parametrized $\boldsymbol{B}_2 + i\boldsymbol{B}_1$ in cyclic basis for the certain chiral state ($\epsilon_H = -\epsilon_T = -1$), for
Repr.	E	3^+	2_a	$\boldsymbol{F}$	$\boldsymbol{B}_2 - i\boldsymbol{B}_1$	$\boldsymbol{B}_2 + i\boldsymbol{B}_1$	which $\boldsymbol{B}_2 - i\boldsymbol{B}_1 = 0$
DT1	$\begin{pmatrix}1&0\\0&1\end{pmatrix}$	$\begin{pmatrix}1&0\\0&1\end{pmatrix}$	$\begin{pmatrix}0&1\\1&0\end{pmatrix}$	$\begin{pmatrix}F\\-F^*\end{pmatrix}_{(0)}$	$\begin{pmatrix}\boldsymbol{B}_2 - i\boldsymbol{B}_1\\(\boldsymbol{B}_2 - i\boldsymbol{B}_1)^*\end{pmatrix}_{(-1)}$	$\begin{pmatrix}\boldsymbol{B}_2 + i\boldsymbol{B}_1\\(\boldsymbol{B}_2 + i\boldsymbol{B}_1)^*\end{pmatrix}_{(+1)}$	$-3S(1+\sin\omega)\begin{pmatrix}e^{i\varphi}\\e^{-i\varphi}\end{pmatrix}_{(+1)}$
DT2	$\begin{pmatrix}1&0\\0&1\end{pmatrix}$	$\begin{pmatrix}a&0\\0&a^*\end{pmatrix}$	$\begin{pmatrix}0&1\\1&0\end{pmatrix}$	$\begin{pmatrix}F\\F^*\end{pmatrix}_{(+1)}$	$\begin{pmatrix}\boldsymbol{B}_2 - i\boldsymbol{B}_1\\-(\boldsymbol{B}_2 - i\boldsymbol{B}_1)^*\end{pmatrix}_{(0)}$	$\begin{pmatrix}\boldsymbol{B}_2 + i\boldsymbol{B}_1\\(\boldsymbol{B}_2 + i\boldsymbol{B}_1)^*\end{pmatrix}_{(-1)}$	$-3S(1-\sin\omega)\begin{pmatrix}e^{-i\varphi}\\e^{i\varphi}\end{pmatrix}_{(-1)}$
DT3	$\begin{pmatrix}1&0\\0&1\end{pmatrix}$	$\begin{pmatrix}a^*&0\\0&a\end{pmatrix}$	$\begin{pmatrix}0&1\\1&0\end{pmatrix}$	$\begin{pmatrix}F\\F^*\end{pmatrix}_{(-1)}$	$\begin{pmatrix}\boldsymbol{B}_2 - i\boldsymbol{B}_1\\(\boldsymbol{B}_2 - i\boldsymbol{B}_1)^*\end{pmatrix}_{(+1)}$	$\begin{pmatrix}\boldsymbol{B}_2 + i\boldsymbol{B}_1\\-(\boldsymbol{B}_2 + i\boldsymbol{B}_1)^*\end{pmatrix}_{(0)}$	$3S\sqrt{2}\cos\omega\begin{pmatrix}1\\-1\end{pmatrix}_{(0)}$

plane ("ferromagnetic" state). Another one, with $\boldsymbol{B}_{1,2} \neq 0$ and $\boldsymbol{F} = \boldsymbol{0}$, represents a triangular helicoidal structure with a 120° phase shift in each plane for the three nonequivalent positions. Note that the symmetry of the system allows for the coexistence of antiferromagnetic and ferromagnetic components. However, such components are determined by the weaker exchange-relativistic interactions. For this reason, in what follows we will omit them.

Taking into account the existing data for the hierarchy of in-plane ($J_{1,2}$) and interplane exchange interactions [14,15], see Fig. 1, we consider the exchange Hamiltonian to specify the magnetic structure and the parameters of the thermodynamic potential (3). Using Fourier components of the spins and expressing them in terms of the order parameters (1), we represent the exchange part of the thermodynamic potential at $T = 0$ (per one magnetic ion) in the form

$$\Phi_{exch} = \frac{4}{9}[(\mathcal{J}_1 + 2\mathcal{J}_2) + (\mathcal{J}_3 + \mathcal{J}_4 + \mathcal{J}_5)\cos k_z]|\boldsymbol{F}|^2 - \frac{1}{9}[(\mathcal{J}_1 + 2\mathcal{J}_2) + (\mathcal{J}_3 + \mathcal{J}_5 - 2\mathcal{J}_4)\cos k_z](|\boldsymbol{B}_1|^2 + |\boldsymbol{B}_2|^2)$$
$$- i\frac{\sqrt{3}}{9}(\mathcal{J}_3 - \mathcal{J}_5)\sin k_z(\boldsymbol{B}_1\boldsymbol{B}_2^* - \boldsymbol{B}_1^*\boldsymbol{B}_2). \quad (4)$$

Here, the exchange energy depends on the order parameters $\boldsymbol{F}$ and $\boldsymbol{B}_{1,2}$ as obtained in Eq. (3), and also on the wave vector $\boldsymbol{k} = (0, 0, k_z)$, the equilibrium value of which should minimize Φ_{exch}. As a result, the helix equilibrium configuration is determined by the angle of rotation k_z along the c axis:

$$\text{tg}k_z = -\frac{\sqrt{3}i(\mathcal{J}_5 - \mathcal{J}_3)(\boldsymbol{B}_1\boldsymbol{B}_2^* - \boldsymbol{B}_1^*\boldsymbol{B}_2)}{(\mathcal{J}_3 + \mathcal{J}_5 - 2\mathcal{J}_4)(|\boldsymbol{B}_1|^2 + |\boldsymbol{B}_2|^2) - 4(\mathcal{J}_3 + \mathcal{J}_4 + \mathcal{J}_5)|\boldsymbol{F}|^2} \approx -\frac{\sqrt{3}(\mathcal{J}_5 - \mathcal{J}_3)}{(\mathcal{J}_3 + \mathcal{J}_5 - 2\mathcal{J}_4)}\epsilon_T. \quad (5)$$

Thus, the values of the exchange interactions $J_1, \ldots, J_5$, and the order parameters determine the wave vector. The wave vector depends on the stability of a particular structure. For instance, the minimum energy for $\boldsymbol{F} \neq \boldsymbol{0}$ and $\boldsymbol{B}_{1,2} = \boldsymbol{0}$ corresponds to a magnetic structure with a wave vector $\boldsymbol{k} = \boldsymbol{0}$. Next, we will discuss another case: $\boldsymbol{F} = \boldsymbol{0}$ and $\boldsymbol{B}_{1,2} \neq \boldsymbol{0}$ and $\boldsymbol{k} \neq \boldsymbol{0}$, which occurs in Fe langasites.

One can consider the spins (magnetic moments) saturated up to the value of S at low temperatures. Then their values,

$$S^2 = |\boldsymbol{S}_\nu(\boldsymbol{k}, \boldsymbol{r}_m)|^2 = \left(\boldsymbol{S}_{\nu\boldsymbol{k}}^+\boldsymbol{S}_{\nu\boldsymbol{k}}''^2\right) + 2\left(\boldsymbol{S}_{\nu\boldsymbol{k}}'^2 - \boldsymbol{S}_{\nu\boldsymbol{k}}''^2\right)\cos(2\boldsymbol{k}\boldsymbol{r}_m) + 2\boldsymbol{S}_{\nu\boldsymbol{k}}'\boldsymbol{S}_{\nu\boldsymbol{k}}''\sin(2\boldsymbol{k}\boldsymbol{r}_m), \quad (6)$$

should be preserved. At such condition, imaginary and real parts of spins are orthogonal, $\boldsymbol{S}_{\nu\boldsymbol{k}}'\boldsymbol{S}_{\nu\boldsymbol{k}}'' = 0$, and their moduli are equal, $\boldsymbol{S}_{\nu\boldsymbol{k}}'^2 = \boldsymbol{S}_{\nu\boldsymbol{k}}''^2 = S^2/2$.

Taking into account that in Fe langasites all exchange interactions are antiferromagnetic ($J_i > 0$) as well as $J_1 + 2J_2 > (J_3 + J_4 + J_5)\cos k_z$ [22,21], one can conclude that the "ferromagnetic" state with $\boldsymbol{F} \neq \boldsymbol{0}$ is energetically unfavorable and the triangular helical structure with $\boldsymbol{B}_{1,2} \neq \boldsymbol{0}$ and $\boldsymbol{F} = \boldsymbol{0}$ is stabilized instead. Considering the constraints on the imaginary and real parts of the spins at low temperatures and the condition $\boldsymbol{F} = \boldsymbol{0}$, one can obtain that imaginary and real parts of the same vectors $\boldsymbol{B}_1$ (or $\boldsymbol{B}_2$) are orthogonal ($\boldsymbol{B}_1'\boldsymbol{B}_1'' = \boldsymbol{B}_2'\boldsymbol{B}_2'' = 0$), as well as vectors of real and imaginary parts of the different $\boldsymbol{B}_1$ and $\boldsymbol{B}_2$ are also orthogonal ($\boldsymbol{B}_1'\boldsymbol{B}_2' = \boldsymbol{B}_1''\boldsymbol{B}_2'' = 0$) [Fig. 2(b)]. This results in the following relationship between $\boldsymbol{B}_1$ and $\boldsymbol{B}_2$: $\boldsymbol{B}_1 = \pm i\boldsymbol{B}_2$ (or $\boldsymbol{B}_1' = \mp\boldsymbol{B}_2''$, $\boldsymbol{B}_1'' = \pm\boldsymbol{B}_2'$), which determines their mutual orientation as well the magnitudes of real and imaginary counterparts: $\boldsymbol{B}_1'^2 = \boldsymbol{B}_1''^2 =$

$\boldsymbol{B}_2'^2 = \boldsymbol{B}_2''^2 = (3S)^2/2$ in such simplified (reduced) magnetic structure.

We specify the above constraints for simple planar magnetic structure in ab^* plane. The order parameters $\boldsymbol{B}_1$ and $\boldsymbol{B}_2$ can be presented in the form $\boldsymbol{B}_2 = -\frac{3S}{2}(\mathbf{u} - i\mathbf{v})$ and $\boldsymbol{B}_1 = \frac{3S}{2} i\epsilon_T(\mathbf{u} - i\mathbf{v})$, where $\mathbf{u} = (1, 0, 0)$ and $\mathbf{v} = (0, 1, 0)$, and parameter $\epsilon_T = \pm 1$ characterizes mutual orientation of $\boldsymbol{B}_1$ and $\boldsymbol{B}_2$ as $\boldsymbol{B}_1 = -i\epsilon_T \boldsymbol{B}_2$. Obviously, for an arbitrarily orientated plane of the magnetic structure, such ratio holds. This enables us to obtain the second (simplified) form of Eq. (5), which was found earlier in [21,23]. For the known values of exchange integrals [21] the energy minimum corresponds to the wave number $k_z \approx \pm 1/7 = (1/7)\epsilon_H$, where ϵ_H characterizes anticlockwise ($\epsilon_H = +1$) or clockwise ($\epsilon_H = -1$) rotation of the spins in helix (helical chirality). For left- and right-handed crystal structures the sign of parameter $\epsilon_{St} = \text{sign}(J_5 - J_3)$ is opposite and can define its structural chirality. Using Eq. (5) for magnetic structure with $\boldsymbol{F} = \mathbf{0}$ and $\boldsymbol{B}_{1,2} \neq \mathbf{0}$ we express helical chirality as $\epsilon_H = -\epsilon_T \epsilon_{St}$, where $\epsilon_T = i(\boldsymbol{B}_1\boldsymbol{B}_2^* - \boldsymbol{B}_1^*\boldsymbol{B}_2)/(|B_1|^2 + |B_2|^2)$.

One can specify the sense of ϵ_T in terms of mutual orientation of neighbor spins in triangular plane structure. According to Eq. (1) and $\boldsymbol{B}_1 = -i\epsilon_T \boldsymbol{B}_2$ the Fourier components of spins are determined only by the vector $\boldsymbol{B}_2 = \boldsymbol{B}_2' + i\boldsymbol{B}_2''$ and take the form $\boldsymbol{S}_{3\boldsymbol{k}} = -\frac{1}{3}\boldsymbol{B}_2$, $\boldsymbol{S}_{1\boldsymbol{k},2\boldsymbol{k}} = -\frac{1}{3}\boldsymbol{B}_2 e^{\pm i\frac{2\pi}{3}\epsilon_T}$, where $\epsilon_T = \pm 1$ represents triangular chirality characterizing anticlockwise (+1) or clockwise spin rotation (–1) in the triangle [Fig. 2(b)], in agreement with [19]. For a crystal in the left-handed enantiomorphic modification ($\epsilon_{St} = +1$), in which $J_5 > J_3$, and the triangular chirality $\epsilon_T = +1$ the helix chirality is $\epsilon_H = -1$, while for $\epsilon_T = -1$ it is $\epsilon_H = +1$. Further, we will use the chirality $\epsilon_T = +1$, $\epsilon_H = -1$, observed earlier by the x-ray and neutron experiments [14,19].

Thus, in exchange approximation, the magnetic structure is characterized by two orthogonal complex vectors, $\boldsymbol{B}_1$ and $\boldsymbol{B}_2$. They determine three magnetic helixes with $\boldsymbol{k} = (0, 0, \epsilon_H k)$ wave vector, with planes parallel to each other and, in general, oriented arbitrarily with respect to the crystal axes. This structure can be characterized by two spherical angles, determining the orientation of one of the four vectors $\boldsymbol{B}_{1,2}'$, $\boldsymbol{B}_{1,2}''$, for example, $\boldsymbol{B}_2' = (3S/\sqrt{2})(\cos\varphi\sin\omega, \sin\varphi\sin\omega, \cos\omega)$. Since $\boldsymbol{B}_2'$ and $\boldsymbol{B}_2''$ are orthogonal ($\boldsymbol{B}_2'\boldsymbol{B}_2'' = 0$), one can choose the phase of the arbitrarily orientated helix so as the imaginary component is placed in the basal plane: $\boldsymbol{B}_2'' = (3S/\sqrt{2})(\sin\varphi, -\cos\varphi, 0)$ while the relative orientation of $\boldsymbol{B}_1$ and $\boldsymbol{B}_2$ is determined by the relation $\boldsymbol{B}_1 = -i\boldsymbol{B}_2$. This structure can be also characterized by the normal to the helixes $\boldsymbol{n}(\varphi', \omega') = \boldsymbol{B}_1 \times \boldsymbol{B}_2^*/|\boldsymbol{B}_1 \times \boldsymbol{B}_2^*| = (\cos\varphi'\sin\omega', \sin\varphi'\sin\omega', \cos\omega')$, where

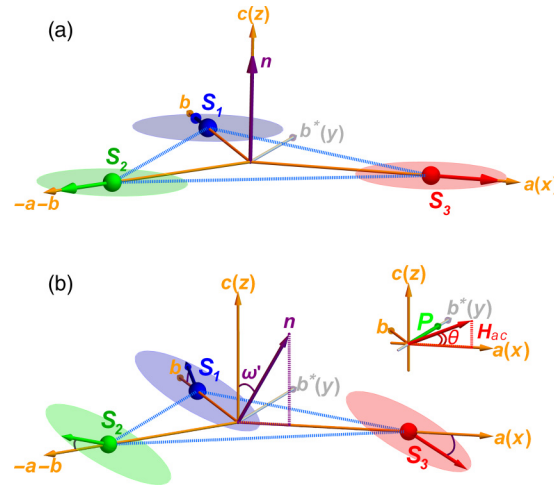

FIG. 8. (a) The ground state of the planar triangular helical magnetic structure in Fe langasites ($\boldsymbol{n}\|\boldsymbol{k}$). Spins $\boldsymbol{S}_1$, $\boldsymbol{S}_2$, and $\boldsymbol{S}_3$ are oriented at angles 120° to each other, and the ellipses indicate planes of the spins' rotation along the c axis. (b) Reorientation of the helix plane and its spin-rotation axis $\boldsymbol{n}$ in magnetic field $\boldsymbol{H}$ lying in the ac plane ($\varphi_H = \pi/2$) at angle θ_H to the ab^* plane. ω' is the deviation of $\boldsymbol{n}$ from the c axis (or the wave vector $\boldsymbol{k}$).

$\omega' = \pi/2 - \omega$ is the deviation of $\boldsymbol{n}$ from the c axis and $\varphi' = \pi + \varphi$ is the deviation of the $\boldsymbol{n}$ projection onto the basal plane from the a axis (Fig. 8). The combinations of order parameter components $B_{1,2}$ in a frame of the reduced description are shown in the last column of Table I in terms of φ and ω angles.

In an external magnetic field, which affects not only the helixes' orientation but also results in their canting and induces a homogeneous magnetization $\boldsymbol{M}$, at least two order parameters, specifically the $\boldsymbol{B}_2'$ (or the normal to the helixes $\boldsymbol{n}$) and magnetization $\boldsymbol{M}$ should characterize the systemreduced description. Due to the relatively weak single-ion anisotropy, we neglect any nonequivalent spin canting in Fe ions' local positions and consider only the total homogeneous magnetization $\boldsymbol{M}$.

B. Thermodynamic potential and magnetic properties

To describe the evolution of the magnetic structure in external magnetic fields, we consider a nonequilibrium thermodynamic potential $\Phi(\boldsymbol{M}, \boldsymbol{F}, \boldsymbol{B}_{1,2})$, which depends on the magnetization $\boldsymbol{M}$ corresponding to the wave vector $k = 0$ and order parameters $\boldsymbol{F}$ and $B_{1,2}$ relating to the wave vector's $\boldsymbol{k} = (0, 0, \pm k)$ group. Taking into account the simplest biquadratic coupling between $\boldsymbol{M}$ and $\boldsymbol{F}$, $B_{1,2}$ it can be represented in the form

$$\Phi(\boldsymbol{M}, \boldsymbol{F}, \boldsymbol{B}_{1,2}) = \Phi_0(\boldsymbol{F}, \boldsymbol{B}_{1,2}) + \frac{A}{2}\boldsymbol{M}^2 + \frac{3D}{2}\sum_{\nu} |\boldsymbol{M}\boldsymbol{S}_{\nu\boldsymbol{k}}|^2 - \boldsymbol{M}\boldsymbol{H} + \cdots$$

$$= \Phi_0(\boldsymbol{F}, \boldsymbol{B}_{1,2}) + \frac{A}{2}\boldsymbol{M}^2 + \frac{D}{2}\left(|\boldsymbol{M}\boldsymbol{F}|^2 + \frac{1}{2}|\boldsymbol{M}\boldsymbol{B}_1|^2 + \frac{1}{2}|\boldsymbol{M}\boldsymbol{B}_2|^2\right) - \boldsymbol{M}\boldsymbol{H} + \cdots, \quad (7)$$

where $\Phi_0(\boldsymbol{F}, \boldsymbol{B}_{1,2})$ is the exchange thermodynamic potential determined by (3); A is the isotropic exchange interaction constant; D takes into account the biquadratic coupling and leads to the dependence of the magnetic helix orientation on $\boldsymbol{M}$ and, consequently, on the magnetic field $\boldsymbol{H}$ (see below).

Minimization of the thermodynamic potential with respect to the magnetization $\boldsymbol{M}$ makes it possible to establish a linear relationship between $\boldsymbol{M}$ and $\boldsymbol{H}$, as well as a nonlinear one with $\boldsymbol{F}$, $\boldsymbol{B}_{1,2}$ in the general case. At low temperatures, when the spins are saturated $[\boldsymbol{B}_1'^2 = \boldsymbol{B}_1''^2 = \boldsymbol{B}_2'^2 = \boldsymbol{B}_2''^2 = (3S)^2/2]$, considering a triangular structure formation ($\boldsymbol{B}_{1,2} \neq 0$ and $\boldsymbol{F} = \boldsymbol{0}$) and the orthogonality condition $\boldsymbol{B}_1 = -i\boldsymbol{B}_2$ fulfilled for vectors $B_{1,2}$, the magnetization $\boldsymbol{M}$ takes the following form:

$$\boldsymbol{M} = \frac{1}{A}\left\{\boldsymbol{H} - \frac{D}{\left(A + D|\boldsymbol{B}_2|^2\right)}[\boldsymbol{B}_2(\boldsymbol{H}\boldsymbol{B}_2^*) + \boldsymbol{B}_2^*(\boldsymbol{H}\boldsymbol{B}_2)]\right\}$$
$$= \frac{1}{A}\left\{\boldsymbol{H} - \frac{2D}{\left(A + D|\boldsymbol{B}_2|^2\right)}\left[\boldsymbol{B}_2'(\boldsymbol{H}\boldsymbol{B}_2') + \boldsymbol{B}_2''\left(\boldsymbol{H}\boldsymbol{B}''_2\right)\right]\right\}, \quad (8)$$

where the second part of the expression is written in terms of real vectors $\boldsymbol{B}_2'$ and $\boldsymbol{B}_2''$, and the sum $\boldsymbol{B}_2^{'}(\boldsymbol{H}\boldsymbol{B}_2^{'}) + \boldsymbol{B}_2''(\boldsymbol{H}\boldsymbol{B}_2'')$ characterizes the plane of the magnetic helix. Thus, depending on the orientation of the field relative to the magnetic helix plane (or orthogonal vectors $\boldsymbol{B}_2'$ and $\boldsymbol{B}_2''$), anisotropy of the magnetization arises. When the field is perpendicular to the helix plane ($\boldsymbol{H} \perp \boldsymbol{B}_2' \perp \boldsymbol{B}_2''$), the susceptibility $\chi_\perp = 1/A$ determines the magnetization $\boldsymbol{M}$, which is related to the magnetic field vector as $\boldsymbol{M} = \chi_\perp \boldsymbol{H}$. When the field lies in the helix plane, the magnetization is also proportional to the magnetic field vector, but it is determined by the parallel susceptibility $\chi_{||} = 1/(A + |B_2|^2 D)$. In both cases, magnetization results from helical structure canting.

Substituting $\boldsymbol{M}$ from Eq. (8) in the thermodynamic potential (7) we arrive to a potential depending only on $\boldsymbol{B}_2$ or its normalized value $\boldsymbol{b}_2 = \boldsymbol{B}_2/(3S)$:

$$\Phi(\boldsymbol{b}_2) = \Phi_0(\boldsymbol{b}_2) - \tfrac{1}{2}\chi_\perp \boldsymbol{H}^2 + \tfrac{1}{2}(\chi_\perp - \chi_{||})|\boldsymbol{H}\boldsymbol{b}_2|^2$$
$$+ \tfrac{1}{2}K|\boldsymbol{c}\boldsymbol{b}_2|^2 + \cdots, \quad (9)$$

where the effective magnetic anisotropy ($K > 0$), which stabilizes the spiral in the basal plane, is added; $\boldsymbol{c} = (0, 0, 1)$ is a unit vector. As we noted above, the real and imaginary parts of the vector $\boldsymbol{b}_2$ are orthogonal and are determined by the angles ω and φ: $\boldsymbol{B}_2' = (1/\sqrt{2})(\cos\varphi\sin\omega, \sin\varphi\sin\omega, \cos\omega)$, $\boldsymbol{B}_2'' = (1/\sqrt{2})(\sin\varphi, -\cos\varphi, 0)$ which also determine an orientation of the normal $\boldsymbol{n} = \boldsymbol{B}_1 \times \boldsymbol{B}_2^*/|\boldsymbol{B}_1 \times \boldsymbol{B}_2^*|$ to the helix plane taking into account that $\boldsymbol{B}_1 = -i\boldsymbol{B}_2$. By minimization of the thermodynamic potential (9) with respect to the angles φ and ω one can obtain for them

$$\mathrm{tg}2\omega = \frac{H^2 \sin 2\theta_H}{H_{sf}^2 - H^2 \cos 2\theta_H}, \quad \varphi = \varphi_H. \quad (10)$$

Here, θ_H is a deviation of the magnetic field from the ab^* plane and Φ_H characterizes the field projection on the ab^* plane relative to the a axis. We note that the magnetic helix deviation ω depends only on the angle θ_H and does not depend on field orientation in the basal plane (Φ_H).

For $H||c$ ($\theta_H = \pi/2$), the helix plane remains in the basal plane (i.e., $\omega = \pi/2$) at any value of the external magnetic field and the magnetization occurs due to canting of the magnetic moments along the field. When the field is in the basal plane ($\theta_H = 0$), a spin-flop transition occurs in field $H_{sf}^2 = K/(\chi_\perp - \chi_{||})$, which is accompanied by the helix reorientation perpendicular to the magnetic field (i.e., $\omega = \pi/2 \rightarrow \omega = 0$). When the field deviates from the basal plane ($\theta_H \neq 0$), the magnetic transition occurs more smoothly and becomes less pronounced, while the spiral plane continuously reorients (Fig. 8), which leads to a decrease in symmetry and inducing of electric polarization. Direct magnetization measurements did not reveal the spin-flop transition perhaps due to the small $\Delta\chi$ and weak magnetic anomaly or a smooth character of the transition. We estimated the value of $H_{sf} \sim 8\,\mathrm{T}$ from a comparison of the experimental and theoretical dependences of the magnetoelectric effect (see below). To do this we calculated orientational dependences of order parameters using the values of parallel and perpendicular susceptibilities, $\chi_{||} \approx 6.6 \times 10^{-5}\,\mathrm{cm}^3/\mathrm{g}$ and $\chi_\perp \approx 6.9 \times 10^{-5}\,\mathrm{cm}^3/\mathrm{g}$, estimated from our magnetic data (Fig. 4).

C. Analysis of magnetoelectric phenomena

As already mentioned, the Fe-langasite space group allows the existence of a magnetoelectric effect, which agrees with experimental results reported in [16,17,26]. Further, we will establish the relationship between the electric polarization and the order parameters based on the symmetry of the system.

To analyze the polarization P_γ, we construct the magnetoelectric part of the thermodynamic potential in a form of quadratic expansion with respect to spins $S_{\nu\alpha}(\boldsymbol{k}, \boldsymbol{r}_m)$ and linear expansion with respect to polarization, similarly to Refs. [35,42], which, after Fourier transformation, can be represented as

$$\Phi_{\mathrm{ME}} = \sum_{\alpha\beta\gamma} c'_{\alpha\beta\gamma} S_{\nu\alpha\boldsymbol{k}} S^*_{\nu\beta\boldsymbol{k}} P_\gamma + \mathrm{c.c.} \quad (11)$$

It is convenient to replace the Fourier spin components with symmetrized order parameters $\boldsymbol{M}$,$\boldsymbol{F}$, $\boldsymbol{B}_{1,2}$.

Table II shows the transformation properties of the magnetization $\boldsymbol{M}$, its quadratic combinations $\boldsymbol{M}^{(2)}$, and polarization $\mathbf{P}$ in the group of the wave vector $\boldsymbol{k}_0 = (0, 0, 0)$. In addition, using transformation properties of the symmetrized spin combinations in the $\boldsymbol{k} = (0, 0, \pm k)$ group from Table I, we constructed the basic quadratic combinations of $\boldsymbol{F}$, $\boldsymbol{B}_1$, and $\boldsymbol{B}_2$, which transform according to the Γ_3 representation of the $\boldsymbol{k}_0$ group (Table II).

As a result, bilinear combinations of polarization components and actual quadratic magnetic order parameters ($\boldsymbol{B}_1{}^{(2)}$, $\boldsymbol{B}_2{}^{(2)}\cdots$) belonging to the same components of the two-dimensional representation allow us to derive the corresponding magnetoelectric contribution in the

TABLE II. Irreducible representations of the $\boldsymbol{k} = 0$ group of the P321 space group and transformation properties of the homogeneous magnetization $\boldsymbol{M}$ ($\boldsymbol{M}_{\pm} = M_x \pm iM_y$), electric polarization $\boldsymbol{P}$ ($P_{\pm} = P_x \pm iP_y$), and quadratic combinations of $\boldsymbol{M}$, as well as quadric combinations of order parameters $\boldsymbol{F}$, $\boldsymbol{B}_{1,2}$ from the $\boldsymbol{k} = (0, 0, \pm k)$ wave vector group, which also realize representations for the $k = 0$ group. The last column represents quadratic combinations of order parameters $\boldsymbol{B}_{1,2}$ in a reduced description (see text).

	Matrices of the representations of the group				Homogeneous magnetization		Quadric combinations of the $\boldsymbol{F}$, $\boldsymbol{B}_1$, and $\boldsymbol{B}_2$ cyclic components		Parametrized quadric combinations of the $\boldsymbol{B}_2 + i\boldsymbol{B}_1$ in cyclic basis for the certain chiral state ($\in_H = -\in_T = -1$), for which
Repr.	E	3^+	2_a	$\boldsymbol{P}$	$\boldsymbol{M}$	$\boldsymbol{M}^{(2)}$	$\boldsymbol{F}^{(2)}$	$\boldsymbol{B}_1^{(2)}; \boldsymbol{B}_2{}^{(2)}$	$\boldsymbol{B}_2 - i\boldsymbol{B}_1 = 0$
Γ_1	1	1	1			$\boldsymbol{M}^2$, M_+M_-, M_z^2	$\lvert\boldsymbol{F}\rvert^2$, $\lvert F_{(+1)}\rvert^2$, $\lvert F_{(-1)}\rvert^2$, $\lvert F_{(0)}\rvert^2$	$\lvert\boldsymbol{B}_1\rvert^2 + \lvert\boldsymbol{B}_2\rvert^2$, $\lvert\boldsymbol{B}_1\rvert^2 + \lvert\boldsymbol{B}_2\rvert^2 \pm i(\boldsymbol{B}_1\boldsymbol{B}_2^* - \boldsymbol{B}_1^*\boldsymbol{B}_2)$ $= \lvert(\boldsymbol{B}_2 \pm i\boldsymbol{B}_1)_{(+1)}\rvert^2 + \lvert(\boldsymbol{B}_2 \pm i\boldsymbol{B}_1)_{(-1)}\rvert^2$ $-\lvert(\boldsymbol{B}_2 \pm i\boldsymbol{B}_1)_{(0)}\rvert^2$	$\lvert\boldsymbol{B}_1\rvert^2 + \lvert\boldsymbol{B}_2\rvert^2 + i(\boldsymbol{B}_1\boldsymbol{B}_2^* - \boldsymbol{B}_1^*\boldsymbol{B}_2)$ $= (3S)^2[2(1+\sin\omega)^2 + 2(1-\sin\omega)^2$ $+4\cos^2\omega] = 4(3S)^2$
Γ_2	1	1	−1	P_z	M_z				
Γ_3	$\begin{pmatrix}1 & 0\\ 0 & 1\end{pmatrix}$	$\begin{pmatrix}a & 0\\ 0 & a^*\end{pmatrix}$	$\begin{pmatrix}0 & 1\\ 1 & 0\end{pmatrix}$	$\begin{pmatrix}P_+\\ P_-\end{pmatrix}$	$\begin{pmatrix}M_+\\ M_-\end{pmatrix}$	$\begin{pmatrix}M_-^2\\ M_+^2\end{pmatrix}$	$\begin{pmatrix}F_{(+1)}^*F_{(-1)}\\ F_{(+1)}F_{(-1)}^*\end{pmatrix}$	$\begin{pmatrix}(\boldsymbol{B}_2 \pm i\boldsymbol{B}_1)_{(-1)}^*(\boldsymbol{B}_2 \pm i\boldsymbol{B}_1)_{(0)}\\ -(\boldsymbol{B}_2 \pm i\boldsymbol{B}_1)_{(-1)}(\boldsymbol{B}_2 \pm i\boldsymbol{B}_1)_{(0)}^*\end{pmatrix}$	$-(3S)^2\sqrt{2}(1-\sin\omega)\cos\omega\begin{pmatrix}e^{i\varphi}\\ -e^{-i\varphi}\end{pmatrix}$
							$\begin{pmatrix}-F_{(0)}^*F_{(+1)}\\ F_{(0)}F_{(+1)}^*\end{pmatrix}$	$\begin{pmatrix}(\boldsymbol{B}_2 \pm i\boldsymbol{B}_1)_{(-1)}(\boldsymbol{B}_2 \pm i\boldsymbol{B}_1)_{(+1)}^*\\ (\boldsymbol{B}_2 \pm i\boldsymbol{B}_1)_{(-1)}^*(\boldsymbol{B}_2 \pm i\boldsymbol{B}_1)_{(+1)}\end{pmatrix}$	$(3S)^2\cos^2\omega\begin{pmatrix}e^{-2i\varphi}\\ e^{2i\varphi}\end{pmatrix}$
						$\begin{pmatrix}M_+M_z\\ -M_-M_z\end{pmatrix}$			
							$\begin{pmatrix}F_{(0)}F_{(-1)}^*\\ -F_{(0)}^*F_{(+1)}\end{pmatrix}$	$\begin{pmatrix}-(\boldsymbol{B}_2 \pm i\boldsymbol{B}_1)_{(0)}^*(\boldsymbol{B}_2 \pm i\boldsymbol{B}_1)_{(+1)}\\ (\boldsymbol{B}_2 \pm i\boldsymbol{B}_1)_{(0)}(\boldsymbol{B}_2 \pm i\boldsymbol{B}_1)_{(+1)}^*\end{pmatrix}$	$(3S)^2\sqrt{2}(1+\sin\omega)\cos\omega\begin{pmatrix}e^{i\varphi}\\ -e^{-i\varphi}\end{pmatrix}$

form

$$\Phi_{\rm ME}(\boldsymbol{b}_1,\boldsymbol{b}_2)=\alpha_1^{(+)}{\rm Im}[P_-(\boldsymbol{b}_2+i\boldsymbol{b}_1)^*_{(-1)}(\boldsymbol{b}_2+i\boldsymbol{b}_1)_{(0)}]-\alpha_2^{(+)}{\rm Im}[P_-(\boldsymbol{b}_2+i\boldsymbol{b}_1)^*_{(0)}(\boldsymbol{b}_2+i\boldsymbol{b}_1)_{(+1)}]$$
$$+\alpha_3^{(+)}{\rm Re}[P_-(\boldsymbol{b}_2+i\boldsymbol{b}_1)_{(-1)}(\boldsymbol{b}_2+i\boldsymbol{b}_1)^*_{(+1)}]+\alpha_1^{(-)}{\rm Im}[P_-(\boldsymbol{b}_2-i\boldsymbol{b}_1)^*_{(-1)}(\boldsymbol{b}_2-i\boldsymbol{b}_1)_{(0)}]$$
$$-\alpha_2^{(-)}{\rm Im}[P_-(\boldsymbol{b}_2-i\boldsymbol{b}_1)^*_{(0)}(\boldsymbol{b}_2-i\boldsymbol{b}_1)_{(+1)}]+\alpha_3^{(-)}{\rm Re}[P_-(\boldsymbol{b}_2-i\boldsymbol{b}_1)_{(-1)}(\boldsymbol{b}_2-i\boldsymbol{b}_1)^*_{(+1)}]+\cdots, \quad (12)$$

where the normalized order $\boldsymbol{b}_{1,2}$ are used, the weak contribution of $\boldsymbol{F}$ is omitted, and $\alpha^{(\pm)}_{1,2,3}$ are phenomenological constants. The terms containing $\alpha^{(\pm)}_{1,2}$ contribute to polarization only when the plane of the magnetic helix deviates from the basal plane (components $B_{1(0)}$ and $B_{2(0)}$). The $\alpha^{(\pm)}_3$ terms include only the in-plane components of the vectors $B_{1,2}$ and can contribute generally even when the helix is in the basal plane, but at low temperatures when the magnetic moments are saturated (see above), this contribution disappears. A similar magnetoelectric interaction, but in a different form, was proposed in [28].

In the reduced description, when the magnetic helix is described by two angles $\varphi=\varphi_H$ and $\omega(\theta_H,H)$ [see Eq. (10)], the $\Phi_{\rm ME}(\boldsymbol{b}_1,\boldsymbol{b}_2)$ is simplified and takes the form:

$$\Phi_{\rm ME}(\varphi_H,\omega)=-\alpha_1^{(+)}\sqrt{2}(1-\sin\omega)\cos\omega[P_x\sin\varphi_H-P_y\cos\varphi_H]+\alpha_2^{(+)}\sqrt{2}(1+\sin\omega)\cos\omega[P_x\sin\varphi_H-P_y\cos\varphi_H]$$
$$+\alpha_3^{(+)}\cos^2\omega[P_x\cos2\varphi_H-P_y\sin2\varphi_H]. \quad (13)$$

Here we suggest for certainty the enantiomorphic crystal modification with $J_5>J_3$ and the triangular chirality $\in_T=+1$ that determines the helix chirality $\in_H=-\in_T\in_{St}=-1$ (see above) for which in the $\Phi_{\rm ME}$ only terms with $\alpha^{(+)}_{1,2,3}$ remain [we omit below the superscript (+) for simplicity]. All terms in Eq. (13) are nonzero only when the helix deviates from the basal plane ($\omega\neq\pi/2$). The first two terms have similar functional dependence on the angle ω, while the third one, quadratic in cosω, is associated with a change only of the $\boldsymbol{B}_1$ and $\boldsymbol{B}_2$ projections on the basal plane.

Similarly, one can derive the magnetoelectric part of the thermodynamic potential associated with the field-induced magnetization $\boldsymbol{M}$. In an external magnetic field, the helix structure becomes canted and nonzero magnetization $\boldsymbol{m}=(m_x,m_y,m_z)$ appears (hereinafter, we use normalized to $M_0=5\mu_bN$ magnetization (8), where N is the number of Fe^{3+} ions). It results in an additional magnetoelectric part of the thermodynamic potential, where we account for quadratic and fourth-power terms on magnetization components:

$$\Phi_{\rm ME}(\boldsymbol{m})=-(\beta_1+\gamma_1\boldsymbol{m}^2)[m_ym_zP_x-m_xm_zP_y]-(\beta_2+\gamma_2\boldsymbol{m}^2)\left[\left(m_x^2-m_y^2\right)P_x-2m_xm_yP_y\right]. \quad (14)$$

When deriving (14), we took into account the definitions of the polarization and the magnetization vector in cyclic coordinates and neglected the slight nonequivalence of Fe ions in C_2 sites due to their weak local anisotropy. As mentioned before, such contributions to the electric polarization were found in rare-earth iron borates [35], aluminum borates [36], and rare-earth langasites [37] also possessing noncentrosymmetric trigonal crystal structure. As to the origin of this magnetoelectric contribution, it could be due to either single-ion anisotropy or Fe-Fe exchange.

As a result, considering the crystal lattice part $P^2/2\chi_{||}{}^E$ of polarization P and minimizing the thermodynamic potential with respect to P, the total equilibrium P_x and P_y components can be represented as

$$\begin{pmatrix}P_x\\P_y\end{pmatrix}=\{[\alpha'_1(1-\sin\omega)-\alpha'_2(1+\sin\omega)]\cos\omega+(\beta'_1+\gamma'_1\boldsymbol{m}^2)m_{||}m_z\}\begin{pmatrix}\sin\varphi_H\\-\cos\varphi_H\end{pmatrix}$$
$$+\{-\alpha'_3\cos^2\omega+(\beta'_2+\gamma'_2\boldsymbol{m}^2)m_{||}^2\}\begin{pmatrix}\cos2\varphi_H\\-\sin2\varphi_H\end{pmatrix}, \quad (15)$$

where $\omega=\omega(\theta_H,H)$ is given by Eq. (10); m_z and $m_{||}$ are magnetization components on the c axis and the basal plane, respectively, determined by Eq. (8); $\chi_{||}{}^E$ is lattice electric susceptibility in the ab^* plane, and $\alpha_{1,2'}=\sqrt{2}\chi_{||}{}^E\alpha_{1,2}$, $\alpha_3{}'=\chi_{||}{}^E\alpha_3\beta_{1,2}{}'=\chi_{||}{}^E\beta_{1,2}$, $\gamma_{1,2}{}'=\chi_{||}{}^E\gamma_{1,2}$.

Below we analyze the polarization in different regimes and determine the magnetoelectric parameters from comparison with experiment (Table III).

In weak fields $H\ll H_{sf}$, the model perfectly describes the orientational dependences of the polarization and its quadratic dependence on H. In such fields, the magnetic helix deviation from the basal plane is small, $\omega\approx\pi/2+(H/H_{sf})^2\sin2\theta_H/2$, as well as the field-quadratic contributions of the induced magnetization $m_{||}m_z\approx\chi_{||}\chi_\perp H^2\cos\theta_H\sin\theta_H/M_0^2$ and $m_{||}{}^2\approx\chi_{||}{}^2H^2\cos^2\theta_H/M_0^2$. As a result, P_x and P_y components of polarization are given by

$$\begin{pmatrix}P_x\\P_y\end{pmatrix}=H^2\sin2\theta_H\left[\alpha'_2\frac{1}{H_{sf}^2}+\beta'_1\frac{\chi_\perp\chi_{||}}{2M_0^2}\right]\begin{pmatrix}\sin\varphi_H\\-\cos\varphi_H\end{pmatrix}+H^2\cos^2\theta_H\beta'_2\frac{\chi_{||}^2}{M_0^2}\begin{pmatrix}\cos2\varphi_H\\-\sin2\varphi_H\end{pmatrix}. \quad (16)$$

Thus, in weak fields, the magnetoelectric effect depends quadratically on the magnetic field value, the polarization changes sign when the magnetic field deviation from the basal plane changes sign [$P(\theta_H)=-P(-\theta_H)$], and the polarization

value is proportional to $\sin 2\theta_H$. This is qualitatively consistent with the experimental dependencies (Fig. 5). The contribution proportional to $\cos^2\theta_H$ in (16) does not manifest itself in weak magnetic fields, but it becomes noticeable in stronger fields, as we discuss in the paragraph below. Only one effective parameter determines the polarization in weak fields, which represents a superposition of contributions from the spiral rotation (α_1') and the induced magnetization (β_1'). As the simulation shows the former is predominant.

Using (8), (10), and (15), we simulated the polarization evolution in fields up to the helix reorientation $H \sim H_{sf}$ (Fig. 6) and determined the phenomenological constants α_1', α_2', and β_1'. A satisfactory description of the field dependence of the polarization is obtained in the geometries $P_{b^*}(H_{a\theta c})$ ($\varphi_H = 0$) and $P_a(H_{a45b^*\theta c})$ ($\varphi_H = \pi/4$) for the following values of magnetoelectric constants $-\alpha_2' =$ –16.1 μC/m^2; $\beta_1' \approx 110\alpha_2' =$ –1760 μC/m^2 [Figs. 6(b) and 6(c)]. In these geometries, there are no contributions from the quadratic terms $-m_\parallel^2(\beta_2' + \gamma_2'\boldsymbol{m}^2)\sin 2\varphi_H$ [or $\sim -m_\parallel^2(\beta_2' + \gamma_2'\boldsymbol{m}^2)\cos 2\varphi_H$, respectively] insensitive to the sign of H_z projection. At a field slightly deviating from the ab^* plane, the polarization remains negligible up to ~4 T, while above this value a sharp increase occurs [Fig. 6(b), nominal angles $\theta_H = +9^\circ$ and -3°, and Fig. 6(c), $\theta_H = \pm 5^\circ$) due to a contribution of the $((\alpha_2' - \alpha_1')\cos\omega$ term in (15) that indicates a rapid reorientation of the helix plane perpendicular to the magnetic field. We notice that the contribution $\beta_1' m_\parallel m_z$ remains small for these geometries.

In Refs. [26,28] the polarization appearance was also associated with the reorientation of the spin spiral. Remarkably, the polarization sign is sensitive not only to crystal chirality, as noted in [28], but also to the direction of the field deviation from the basal plane (Figs. 5 and 6). To explain the polarization behavior, it is enough to account for the spiral plane rotation without an additional long-wave modulation.

Taking into account the relationship between the spin-rotation axis $\boldsymbol{n}(\varphi', \omega')$ and the vector $B_2'(\varphi, \omega)$ (see above), one can represent the contribution $((\alpha_1' - \alpha_2')\cos\omega$ as $\boldsymbol{P} \sim \boldsymbol{n} \times \boldsymbol{k}$ and assign it to the inverse Dzyaloshinskii-Moriya interaction. At large deviations of the field from the ab^* plane ($\theta_H \sim \pm 45^\circ$), the magnetic helix reorientation becomes noticeable already at weak fields, which explains the observed quadratic increase of the polarization up to ~5 T (Figs. 5(c) and 6, $\theta_H = \pm 45^\circ$). However, in fields exceeding 5 T, the polarization character changes, and its increase slows down. This is due to the contribution from the induced magnetization $\beta_1' m_\parallel m_z$, which is maximal for the $\theta_H = \pm 45^\circ$ and has sign opposite to the contribution from the helix reorientation.

In the geometry $P_a(H_{b^*\theta c})$ ($\varphi_H = \pi/2$) and fields above 5 T, there is an additional quadratic contribution $\beta_2' m_\parallel^2$, which does not depend on the sign of the magnetic field deviation and violates the relation $P(\theta_H) = -P(-\theta_H)$. It manifests itself at small deviation angles [Fig. 6(a), nominal angles $\theta_H = +9^\circ$ and -3°] and makes the polarization $P_a(H)$ behavior different from the $P_b(H)$ one, where this contribution is absent [Figs. 6(a) and 6(b)]. Such additional contribution, as well as the ones associated with a large induced magnetization, is more clearly manifested in pulsed fields when the magnetic helix is reoriented perpendicular to the field direction.

TABLE III. Phenomenological parameters of the magnetoelectric coupling in (15) found by fitting experimental data in fields up to 60 T.

Constant	(μC/m^2)
α_1'	–16
α_2'	16
α_3'	0
β_1'	–1760
γ_1'	3000
β_2'	–750
γ_2'	576

Using the found parameters α_1', α_2', and β_1', we extended the simulation of the polarization up to high pulsed fields $H > H_{sf}$ (Fig. 7) and determined other magnetoelectric constants α_3', β_2', γ_1', and γ_2' (Table III).

In the geometry $P_a(H_{a45b^*\pm 45c})$, when the field projection lies along the ab^*-plane diagonal ($\varphi_H = 45^\circ$), the polarization is given by $P_a = [(\alpha_1' - \alpha_2')\cos\omega + m_{||} m_z(\beta_1' + \gamma_1'\boldsymbol{m}^2)]\sin\varphi_H$ and the relation $P(\theta_H) \approx -P(-\theta_H)$ is valid within the entire range of the fields [Fig. 7(c)]. The polarization value reaches extremum in field ~10 T, where the derivative of the polarization changes sign. This behavior is owing to the opposite signs of the contributions from the helix plane reorientation $(\alpha_1' - \alpha_2')\cos\omega$ and a field-induced magnetization $\beta_1' m_\parallel m_z$. However, the behavior of the polarization changes again in field ~40 T due to the contribution from higher-(fourth-) order terms $\gamma_1' m_{||} m_z \boldsymbol{m}^2$ [Fig. 7(c)] which slows down polarization increase. It is important that the contribution $m_{||} m_z(\beta_1' + \gamma_1'\boldsymbol{m}^2)$ has the maximum value when the magnetic field is oriented at $\theta_H \sim \pm 45^\circ$, and it becomes much weaker at small deviations from the ab^* plane.

In the $P_a(H_{b^*\theta c})$ geometry, the polarization behavior is qualitatively different from the previous case [see Fig. 7(a)] due to the quadratic contribution ${m_{||}}^2\,\beta_2' \cos 2_{\varphi H}$ and an additional fourth-order contribution $\gamma_2'\boldsymbol{m}^2{m_{||}}^2\cos 2\varphi_H$ (taking place above 40 T) which are insensitive to the sign of the field projection on the c axis. In another geometry, $P_a(H_{a45b^*\pm 10c})$ ($\varphi_H = 45^\circ$), the ratio $P(\theta_H) \approx -P(-\theta_H)$ should be valid in the entire range of the fields used, but we did not observe it in the experiment [Fig. 7(b)]. We suppose that field deviation from $\varphi_H = 45^\circ$ can lead to the above-mentioned additional contributions, which violates this ratio. Modeling shows that the contributions occur for small field projection deviations (~5°) from the diagonal of the ab^* plane, which is within the accuracy of the sample's orientation in the experiment.

In a whole, the performed analysis and simulation of the polarization field dependences made it possible to describe the experiment qualitatively and partially quantitatively and to establish the main mechanisms determining the behavior polarization depending on the magnetic structure changes in a wide range of fields.

V. CONCLUSION

We performed a complex experimental and theoretical study of the magnetoelectric effect in Fe langasites possessing

double chiral spin structure in external magnetic fields up to 60 T and elucidated the key features of the field-induced electric polarization as a function of the magnetic field orientation. A sharp increase of transverse $P_a(H_{b^*})$ and $P_{b*}(H_a)$ electric polarizations takes place at fields exceeding the critical field, which is associated with the reorientation of the spin helix plane from the basal plane to a direction perpendicular to the field. At weak to medium fields (up to 8 T), the polarization sign is determined by the direction of the field deviation from the basal plane. It was found experimentally that the polarization behavior changes at fields above 10 T, which is explained by considering additional contributions from field-induced magnetization.

A detailed group-theoretical analysis of the magnetic and magnetoelectric properties of Fe langasites was performed and the interrelation of the polarization and magnetic order parameters in an external magnetic field was established. In the exchange approximation, a reduced description of an arbitrarily orientated magnetic helix structure was proposed through its main (exchange) order parameters. Within this model, two angles characterize the orientation of the magnetic helix plane, and the magnetization vector $\boldsymbol{M}$ determines its canting in the magnetic field. It is shown that the spiral magnetic structure is rotated and canted (analogous to a spin-flop transition) in a magnetic field.

For a wide range of magnetic field strengths and geometries, the experimental data on the magnetoelectric effect are consistently described. At weak fields (up to 8 T), the main contribution to polarization is associated with the magnetic helix reorientation perpendicular to the field. In this case, the field deviation from the basal plane determines the direction of the helix rotation. A sharp polarization increase found at fields up to 8 T and close to the basal plane may indicate a contribution of the inverse Dzyaloshinskii-Moriya interaction. Observed changes in the electric polarization behavior at strong fields (above 10 T) are explained by helix canting and contributions from the symmetry-allowed magnetoelectric terms including field-induced magnetization, possibly originating from a single-ion anisotropy or Fe-Fe exchange interactions.

Note that both of these mechanisms act in a noncentrosymmetric crystal, in which intracrystalline interactions in each enantiomorphic state (inversion twin) set the direction of electric polarization. Therefore, in such crystals, the effect of an external electric field on polarization (i.e., traditional poling, effective in multiferroics with a cycloidal spin structure in centrosymmetric crystals such as, for example, manganites $RMnO_3$, tungstates $MnWO_4$, etc.) is suppressed. At the same time, one cannot completely exclude the possible effect of an electric field on spontaneous electric polarization in noncentrosymmetric crystals. Although we did not find spontaneous polarization in the Fe langasites within experimental accuracy, its existence in the easy plane phase is not forbidden by symmetry, as follows from our analysis [see the third term in Eq. (12) for magnetoelectric energy]. As the preliminary analysis shows, spontaneous polarization can appear in an elliptical spiral structure (but not in a circular one) due to the single-ion anisotropy of Fe^{3+} spins in three local positions (2_a symmetries), as well as the existence of higher-order harmonics in the spin distribution already observed in [22]. The anharmonicity in the spin distribution was also observed in the classical cycloidal multiferroic $BiFeO_3$, by nuclear magnetic resonance [43,44] and by neutron diffraction [45], and found to be responsible for the interaction of higher-order spin wave branches with the *ac* electric field [46]. In the studied Fe langasites the anharmonicity in the spiral spin distribution should only weakly affect static magnetoelectric properties and hence requires high precision experiments to be detected, as well as more sophisticated theoretical analysis.

ACKNOWLEDGMENTS

We acknowledge support from HLD at HZDR (Drezden, Germany), a member of the European Magnetic Field Laboratory, for the high magnetic field experiments. We are very grateful to Virginie Simonet and Evan Constable for fruitful discussions. This work was supported by the Russian Science Foundation (Project No. 16-12-10531).

[1] M. Lines and A. Glass, *Principles and Applications of Ferroelectrics and Related Materials* (Clarendon Press, New York, 1977).

[2] N. A. Hill, Why are there so few magnetic ferroelectrics? J. Phys. Chem. B **104**, 6694 (2000).

[3] T. Kimura, T. Goto, H. Shintani, K. Ishizaka, T. Arima, and Y. Tokura, Magnetic control of ferroelectric polarization, Nature (London) **426**, 55 (2003).

[4] W. Eerenstein, N. D. Mathur, and J. F. Scott, Multiferroic and magnetoelectric materials, Nature (London) **442**, 759 (2006).

[5] Y. Tokura, S. Seki, and N. Nagaosa, Multiferroics of spin origin, Rep. Prog. Phys. **77**, 76501 (2014).

[6] M. Fiebig, Revival of the magnetoelectric effect, J. Phys. D; Appl. Phys. **38**, R123 (2005).

[7] S.-W. Cheong and M. Mostovoy, Multiferroics: A magnetic twist for ferroelectricity, Nat. Mater. **6**, 13 (2007).

[8] Y. Tokura and S. Seki, Multiferroics with spiral spin orders, Adv. Mater. **22**, 1554 (2010).

[9] B. B. Van Aken, T. T. M. Palstra, A. Filippetti, and N. A. Spaldin, The origin of ferroelectricity in magnetoelectric $YMnO_3$, Nat. Mater. **3**, 164 (2004).

[10] B. A. Maksimov, V. N. Molchanov, B. V. Mill, E. L. Belokoneva, M. K. Rabadanov, A. A. Pugacheva, Y. V. Pisarevskii, and V. I. Simonov, Absolute structure of $La_3Ga_5SiO_4$ langasite crystals, Crystallogr. Rep. **50**, 751 (2005).

[11] J. Bohm, R. B. Heimann, M. Hengst, R. Roewer, and J. Schindler, Czochralski growth and characterization of piezoelectric single crystals with langasite structure:

La_3Ga_5SiO (LGS), $La_3Ga_{5.5}Nb_{0.5}O_{14}$ (LGN), and $La_3Ga_{5.5}Ta_{0.5}O_{14}$ (LGT), J. Cryst. Growth **204**, 128 (1999).

[12] J. Sato, H. Takeda, H. Morikoshi, K. Shimamura, P. Rudolph, and T. Fukuda, Czochralski growth of RE_3Ga_5SiO (RE = La, Pr, Nd) single crystals for the analysis of the influence of rare earth substitution on piezoelectricity, J. Cryst. Growth **191**, 746 (1998).

[13] T. Iwataki, H. Ohsato, K. Tanaka, H. Morikoshi, J. Sato, and K. Kawasaki, Mechanism of the piezoelectricity of langasite based on the crystal structures, J. Eur. Ceram. Soc. **21**, 1409 (2001).

[14] K. Marty, V. Simonet, E. Ressouche, R. Ballou, P. Lejay, and P. Bordet, Single Domain Magnetic Helicity and Triangular Chirality in Structurally Enantiopure $Ba_3NbFe_3Si_2O_{14}$, Phys. Rev. Lett. **101**, 247201 (2008).

[15] K. Marty, P. Bordet, V. Simonet, M. Loire, R. Ballou, C. Darie, J. Kljun, P. Bonville, O. Isnard, P. Lejay, B. Zawilski, and C. Simon, Magnetic and dielectric properties in the langasite-type compounds: $A_3BFe_3D_2O_{14}$ (A = Ba, Sr, Ca; B = Ta, Nb, Sb; D = Ge, Si), Phys. Rev. B **81**, 054416 (2010).

[16] N. Lee, Y. J. Choi, and S. W. Cheong, Magnetic control of ferroelectric polarization in a self-formed single magnetoelectric domain of multiferroic $Ba_3NbFe_3Si_2O_{14}$, Appl. Phys. Lett. **104**, 072904 (2014).

[17] H. D. Zhou, L. L. Lumata, P. L. Kuhns, A. P. Reyes, E. S. Choi, N. S. Dalal, J. Lu, Y. J. Jo, L. Balicas, J. S. Brooks, and C. R. Wiebe, $Ba_3NbFe_3Si_2O_{14}$: A new multiferroic with a 2D triangular Fe^{3+} motif, Chem. Mater. **21**, 156 (2009).

[18] S. A. Pikin and I. S. Lyubutin, Phenomenological model of multiferroic properties in langasite-type crystals with a triangular magnetic lattice, Phys. Rev. B **86**, 064414 (2012).

[19] N. Qureshi, A. Bombardi, S. Picozzi, P. Barone, E. Lelièvre-Berna, X. Xu, C. Stock, D. F. McMorrow, A. Hearmon, F. Fabrizi, P. G. Radaelli, S.-W. Cheong, and L. C. Chapon, Absolute crystal and magnetic chiralities in the langasite compound $Ba_3NbFe_3Si_2O_{14}$ determined by polarized neutron and x-ray scattering, Phys. Rev. B **102**, 054417 (2020).

[20] K. Marty, V. Simonet, P. Bordet, R. Ballou, P. Lejay, O. Isnard, E. Ressouche, F. Bourdarot, and P. Bonville, Magnetic characterization of the non centrosymmetric $Ba_3NbFe_3Si_2O_{14}$ langasite, J. Magn. Magn. Mater. **321**, 1778 (2009).

[21] C. Stock, L. C. Chapon, A. Schneidewind, Y. Su, P. G. Radaelli, D. F. McMorrow, A. Bombardi, N. Lee, and S. W. Cheong, Helical spin waves, magnetic order, and fluctuations in the langasite compound $Ba_3NbFe_3Si_2O_{14}$, Phys. Rev. B **83**, 104426 (2011).

[22] L. Chaix, R. Ballou, A. Cano, S. Petit, S. De Brion, J. Ollivier, L. P. Regnault, E. Ressouche, E. Constable, C. V. Colin, A. Zorko, V. Scagnoli, J. Balay, P. Lejay, and V. Simonet, helical bunching and symmetry lowering inducing multiferroicity in Fe langasites, Phys. Rev. B **93**, 214419 (2016).

[23] J. Jensen, Chiral spin-wave excitations of the spin-52 trimers in the langasite compound $Ba_3NbFe_3Si_2O_{14}$, Phys. Rev. B **84**, 104405 (2011).

[24] V. Scagnoli, S. W. Huang, M. Garganourakis, R. A. de Souza, U. Staub, V. Simonet, P. Lejay, and R. Ballou, Dzyaloshinskii-Moriya driven helical-butterfly structure in $Ba_3NbFe_3Si_2O_{14}$, Phys. Rev. B **88**, 104417 (2013).

[25] C. Lee, E. Kan, H. Xiang, and M. H. Whangbo, Theoretical investigation of the magnetic structure and ferroelectric polarization of the multiferroic langasite $Ba_3NbFe_3Si_2O_{14}$, Chem. Mater. **22**, 5290 (2010).

[26] H. Narita, Y. Tokunaga, A. Kikkawa, Y. Taguchi, Y. Tokura, and Y. Takahashi, Observation of nonreciprocal directional dichroism via electromagnon resonance in a chiral-lattice helimagnet $Ba_3NbFe_3Si_2O_{14}$, Phys. Rev. B **94**, 094433 (2016).

[27] H. Katsura, N. Nagaosa, and A. V. Balatsky, Spin Current and Magnetoelectric Effect in Noncollinear Magnets, Phys. Rev. Lett. **95**, 057205 (2005).

[28] M. Ramakrishnan, E. Constable, A. Cano, M. Mostovoy, J. S. White, N. Gurung, E. Schierle, S. de Brion, C. V. Colin, F. Gay, P. Lejay, E. Ressouche, E. Weschke, V. Scagnoli, R. Ballou, V. Simonet, and U. Staub, Field-induced double spin spiral in a frustrated chiral magnet, npj Quantum Mater. **4**, 1 (2019).

[29] A. M. Balbashov and S. K. Egorov, Apparatus for growth of single crystals of oxide compounds by floating zone melting with radiation heating, J. Cryst. Growth **52**, 498 (1981).

[30] A. P. Dudka, A. M. Balbashov, and I. S. Lyubutin, Growth and x-ray diffraction study and specific features of thermal expansion of $Ba_3NbFe_3Si_2O_{14}$ single crystal from the langasite family, Cryst. Growth Des. **16**, 4943 (2016).

[31] H. Mitamura, S. Mitsuda, S. Kanetsuki, H. A. Katori, T. Sakakibara, and K. Kindo, Pyroelectric measurements on a geometrically frustrated spin system CuFeO2 in pulsed high magnetic fields, J. Phys.: Conf. Ser. **51**, 557 (2006).

[32] C. Jia, S. Onoda, N. Nagaosa, and J. H. Han, Bond electronic polarization induced by spin, Phys. Rev. B **74**, 224444 (2006).

[33] C. Jia, S. Onoda, N. Nagaosa, and J. H. Han, Microscopic theory of spin-polarization coupling in multiferroic transition metal oxides, Phys. Rev. B **76**, 144424 (2007).

[34] T. H. Arima, Ferroelectricity induced by proper-screw type magnetic order, J. Phys. Soc. Jpn. **76**, 1 (2007).

[35] A. K. Zvezdin, S. S. Krotov, A. M. Kadomtseva, G. P. Vorob'ev, Y. F. Popov, A. P. Pyatakov, L. N. Bezmaternykh, and E. A. Popova, Magnetoelectric effects in gadolinium iron borate $GdFe_3(BO_3)_4$, J. Exp. Theor. Phys. Lett. **81**, 272 (2005).

[36] V. Y. Ivanov, A. M. Kuzmenko, and A. A. Mukhin, Magnetoelectric effect in ytterbium aluminum borate $YbAl_3(BO_3)_4$, JETP Lett. **105**, 435 (2017).

[37] L. Weymann, L. Bergen, T. Kain, A. Pimenov, A. Shuvaev, E. Constable, D. Szaller, B. V. Mill, A. M. Kuzmenko, V. Y. Ivanov, N. V. Kostyuchenko, A. I. Popov, A. K. Zvezdin, A. Pimenov, A. A. Mukhin, and M. Mostovoy, Unusual magnetoelectric effect in paramagnetic rare-earth langasite, npj Quantum Mater. **5**, 61 (2020).

[38] T. Nagamiya, Helical spin ordering—1 Theory of helical spin configurations, Solid State Phys. **20**, 305 (1968).

[39] D. H. Lyons and T. A. Kaplan, Method for determining ground-state spin configurations, Phys. Rev. **120**, 1580 (1960).

[40] D. A. Varshalovich, A. N. Moskalev, and V. K. Khersonskii, *Quantum Theory of Angular Momentum* (World Scientific, Singapore, 1988).

[41] L. Elcoro, B. Bradlyn, Z. Wang, M. G. Vergniory, J. Cano, C. Felser, B. A. Bernevig, D. Orobengoa, G. de la Flor,

and M. I. Aroyo, Double crystallographic groups and their representations on the Bilbao Crystallographic Server, J. Appl. Crystallogr. **50**, 1457 (2017).

[42] A. B. Harris, Landau analysis of the symmetry of the magnetic structure and magnetoelectric interaction in multiferroics, Phys. Rev. B **76**, 054447 (2007).

[43] A. V. Zalesskiĭ, A. A. Frolov, A. K. Zvezdin, A. A. Gippius, E. N. Morozova, D. F. Khozeev, A. S. Bush, and V. S. Pokatilov, Effect of spatial spin modulation on the relaxation and NMR frequencies of ^{57}Fe nuclei in a ferroelectric antiferromagnet $BiFeO_3$, J. Exp. Theor. Phys. **95**, 101 (2002).

[44] A. A. Bush, A. A. Gippius, A. V. Zalesskii, and E. N. Morozova, ^{209}Bi NMR spectrum of $BiFeO_3$ in the presence of spatial modulation of hyperfine fields, J. Exp. Theor. Phys. Lett. **78**, 389 (2003).

[45] M. Ramazanoglu, W. Ratcliff, Y. J. Choi, S. Lee, S. W. Cheong, and V. Kiryukhin, Temperature-dependent properties of the magnetic order in single-crystal $BiFeO_3$, Phys. Rev. B **83**, 174434 (2011).

[46] R. de Sousa and J. E. Moore, Optical coupling to spin waves in the cycloidal multiferroic $BiFeO_3$, Phys. Rev. B **77**, 012406 (2008).